Title

Indole-3-Propionic Acid Protects Against Heart Failure With Preserved Ejection Fraction.

Journal

Circulation Research, 134(4)

Authors

Wang, Yu-Chen
Koay, Yen
Pan, Calvin
et al.

Publication Date

2024-02-16

DOI

10.1161/CIRCRESAHA.123.322381

Peer reviewed

HHS Public Access

Author manuscript

Circ Res. Author manuscript; available in PMC 2025 February 16.

Published in final edited form as:

Circ Res. 2024 February 16; 134(4): 371–389. doi:10.1161/CIRCRESAHA.123.322381.

Indole-3-Propionic Acid Protects Against Heart Failure with Preserved Ejection Fraction

Yu-Chen Wang[1], **Yen Chin Koay**[2,3], **Calvin Pan**[1], **Zhiqiang Zhou**[1], **W. H. Wilson Tang**[4], **Jennifer Wilcox**[5], **Xinmin S. Li**[5], **Alexia Zagouras**[6], **Francine Marques**[7], **Hooman Allayee**[8], **Federico E Rey**[9], **David M. Kaye**[10,11], **John F. O'Sullivan**[2,3,12,13], **Stanley L. Hazen**[4,5], **Yang Cao**[14,15,*], **Aldons J. Lusis**[1,*]

[1]Department of Medicine, Division of Cardiology, Department of Microbiology, Immunology and Molecular Genetics, and Department of Human Genetics, University of California, Los Angeles, CA, USA.

[2]Cardiometabolic Medicine, School of Medical Sciences, Faculty of Medicine and Health, The University of Sydney, New South Wales, Australia.

[3]Charles Perkins Centre, Sydney, New South Wales, Australia.

[4]Department of Cardiovascular Medicine, Heart, Vascular and Thoracic Institute, Cleveland Clinic, Cleveland OH.

[5]Department of Cardiovascular and Metabolic Sciences, Lerner Research Institute, Cleveland Clinic, Cleveland OH.

[6]Stanford Department of Medicine, Stanford CA, USA.

[7]School of Biological Sciences, Faculty of Medicine, Monash University, Clayton, VIC, Australia.

[8]Department of Preventive Medicine and Institute for Genetic Medicine, University of Southern California Keck School of Medicine, Los Angeles, CA 90089-9075, USA.

[*]Corresponding Author: Aldons J. Lusis (jlusis@mednet.ucla.edu), and Yang Cao (yangcao208@ustc.edu.cn).

Contributions

We thank Dr. Rita M. Cantor for the help with statistical and bioinformatic analyses. Y.C.W., Y.C., and A.J.L. designed the experiments. Y.C.W., Y.C., Y.C.K., Z.Z., Y. M., and S.C., performed the experiments. Y.C.W., Y.C., Y.C.K., and C.P. analyzed raw data. W.H.W.T. and S.L.H. conceived and designed the Cleveland Clinic HFpEF study. J.W. and A.Z. recruited Cleveland Clinic HFpEF subjects. X.S.L. performed statistical analysis of Cleveland Clinic HFpEF study. D.M.K and F.M. performed and analyzed the Alfred Hospital HFpEF study. J.F.O., H.A., F. R. and A.J.L. reviewed the data and made substantial contributions to improving the studies. Y.C.W., Y.C., and A.J.L. wrote the manuscript, which was reviewed by all authors.

Disclosures

Competing interests

Dr. Tang is a consultant for Sequana Medical A.V., Cardiol Therapeutics Inc, Genomics plc, Zehna Therapeutics Inc, Renovacor Inc, and has received honorarium from Springer Nature for authorship/editorship and American Board of Internal Medicine for exam writing committee. Dr. Hazen reports being named as co-inventors on pending and issued patents held by the Cleveland Clinic relating to cardiovascular diagnostics and therapeutics. Dr. Hazen reports having received royalty payments for inventions or discoveries related to cardiovascular diagnostics or therapeutics from Cleveland Heart Lab, a fully owned subsidiary of Quest Diagnostics, and Procter & Gamble. Dr. Hazen is a paid consultant for Zehna Therapeutics and Proctor & Gamble, and has received research funds from Zehna Therapeutics, Proctor & Gamble, Pfizer Inc., and Roche Diagnostics.

Supplemental Material

Expanded Materials and Methods

Supplemental Tables 1–5

Supplemental Figures 1–21

References 62–78

[9]Department of Bacteriology, University of Wisconsin-Madison, Madison, WI, USA.

[10]Baker Heart & Diabetes Institute, Melbourne, Australia.

[11]Department of Cardiology, Alfred Hospital, Melbourne, Australia.

[12]Department of Cardiology, Royal Prince Alfred Hospital, New South Wales, Australia.

[13]Faculty of Medicine, TU Dresden, Germany.

[14]Department of Cardiology, the First Affiliated Hospital of USTC, Division of Life Sciences and Medicine, University of Science and Technology of China, Hefei, Anhui 230001, China.

[15]School of Basic Medical Sciences, Division of Life Sciences and Medicine, University of Science and Technology of China, Hefei, Anhui 230027, China.

Abstract

Background—Heart failure (HF) with preserved ejection fraction (HFpEF) is a common but poorly understood form of HF, characterized by impaired diastolic function. It is highly heterogeneous with multiple comorbidities, including obesity and diabetes, making human studies difficult.

Methods—Metabolomic analyses in a mouse model of HFpEF showed that levels of indole-3-propionic acid (IPA), a metabolite produced by gut bacteria from tryptophan, were reduced in the plasma and heart tissue of HFpEF mice as compared to controls. We then examined the role of IPA in mouse models of HFpEF as well as two human HFpEF cohorts.

Results—The protective role and therapeutic effects of IPA were confirmed in mouse models of HFpEF using IPA dietary supplementation. IPA attenuated diastolic dysfunction, metabolic remodeling, oxidative stress, inflammation, gut microbiota dysbiosis, and intestinal epithelial barrier damage. In the heart, IPA suppressed the expression of nicotinamide N-methyl transferase (NNMT), restored nicotinamide, NAD^+/NADH, and SIRT3 levels. IPA mediates the protective effects on diastolic dysfunction, at least in part, by promoting the expression of SIRT3. SIRT3 regulation was mediated by IPA binding to the aryl hydrocarbon receptor (AhR), as *Sirt3* knockdown diminished the effects of IPA on diastolic dysfunction in vivo. The role of the NAD-NAM circuit in HFpEF was further confirmed by nicotinamide supplementation, *Nnmt* knockdown and *Nnmt* overexpression in vivo. IPA levels were significantly reduced in HFpEF patients in two independent human cohorts, consistent with a protective function in humans as well as mice.

Conclusions—Our findings reveal that IPA protects against diastolic dysfunction in HFpEF by enhancing the NAD salvage pathway, suggesting the possibility of therapeutic management by either altering the gut microbiome composition or supplementing the diet with IPA.

Graphical Abstract

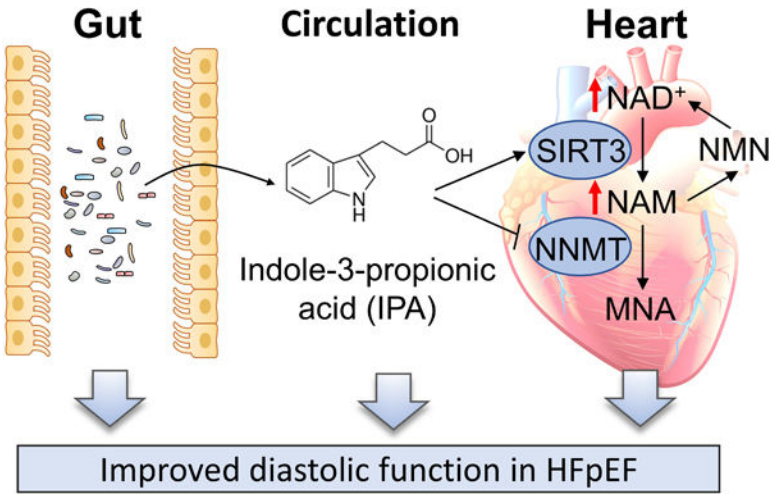

Subject Terms:

Animal Models of Human Disease; Heart Failure

Keywords

Indole-3-propionic acid; HFpEF; nicotinamide; NAD^+; diastolic dysfunction; metabolic remodeling; AhR

Introduction

HFpEF is an increasingly prevalent disorder that accounts for half of all cases of heart failure [1–3]. It is characterized by diastolic dysfunction and preserved ejection fraction, distinct from heart failure with reduced ejection fraction (HFrEF) [1–3]. Unlike the proven therapies for HFrEF, trials of traditional heart failure medications have been unsuccessful in HFpEF and, to date, only the sodium-glucose cotransporter 2 (SGLT2) inhibitor, dapagliflozin, has been shown to improve symptoms in chronic HFpEF [1, 4–7].

HFpEF is a complex disorder with multiple comorbidities, including obesity, diabetes, and hypertension [8, 9]. It is highly heterogeneous and driven in large part by environmental factors, making human studies difficult. To enable genetic and molecular analysis, we have used a mouse model of the disorder developed by Schiattarella and colleagues [10]. It involves feeding mice a high-fat diet and a nitric oxide synthase inhibitor. By metabolic profiling of heart tissue in the HFpEF mouse model, we found that indole-3-propionic acid (IPA), a metabolite synthesized by the gut microbe from dietary tryptophan [11–13], was considerably decreased in both heart tissue and circulation as compared to a regular diet.

Tryptophan is an essential amino acid which plays a vital role in maintaining proper physiological balance through its biologically active compounds, including serotonin, tryptamine, NAD^+, kynurenines, and indoles [14, 15]. In the gut, dietary tryptophan can be converted into IPA by bacteria such as *Lactobacillus reuteri, Akkermansia muciniphila* and

Clostridium sporogenes [16–19]. IPA has been found to bind to its receptors and preserve mucosal homeostasis and gastrointestinal barrier function [20]. In addition to the gut, IPA also modulates mitochondrial function and enhances metabolic activity in several tissues [21, 22]. In human populations, elevated plasma concentrations of IPA have been correlated with a reduced risk of type 2 diabetes [23, 24].

Here we report that the decrease of IPA levels is accompanied by metabolic remodeling, gut dysbiosis, increased oxidative stress and inflammation in the heart of HFpEF mice. IPA feeding increased IPA levels in the heart and circulation and attenuated diastolic dysfunction induced by the HFpEF diet. IPA also mitigated gut microbiota dysbiosis and intestinal epithelial barrier damage, and improved metabolic homeostasis. In the hearts of HFpEF mice, IPA restored the expression of SIRT3 by aryl hydrocarbon receptor (AhR) binding, and it decreased inflammation and NNMT levels, increasing nicotinamide and NAD^+/NADH. Increased levels of both NAD^+ and SIRT3 have previously been associated with improved diastolic function [25, 26]. To determine whether our findings in the HFpEF model are relevant to humans, we examined two separate cohorts of heart failure patients with HFpEF. Indeed, in both cohorts, the levels of IPA were significantly reduced in HFpEF patients. Together, these data identify IPA as a critical regulator of diastolic dysfunction in HFpEF by enhancing the NAD salvage pathway, and they suggest that IPA supplementation may be effective in therapeutic management of HFpEF.

Methods

Data Availability

All data associated with this study are presented in the article or Supplemental Material. Detailed materials and methods are provided in the Supplemental Material.

Microbiome sequencing data were deposited to BioProject under the accession number PRJNA841683. Results of metabolomics and the R scripts used to perform the heatmap and PCA plot in Figures 2,4, Figure S4 and Figure S11 are available at https://github.com/yangcao208/IPA. The single cell sequencing data generated during this study will be available at the public repository GEO through accession number GSE243718. Any additional information and data supporting this study are available from the corresponding authors upon request.

Results

HFpEF mice exhibit metabolic remodeling which is associated with diastolic dysfunction

To investigate the metabolic remodeling of HFpEF, we first reproduced the “two-hit” HFpEF model in C57BL/6J male and female mice by the combination of high-fat diet (HFD) and inhibition of nitric oxide synthase using Nω-nitrol-arginine methyl ester (l-NAME) [10]. After 7 weeks feeding of HFD + l-NAME feeding, male mice exhibited heart failure phenotypes that recapitulate clinical symptoms of HFpEF, which include diastolic dysfunction (increased E/A ratio, and E/e’ ratio), cardiac hypertrophy, lung congestion, LV (left ventricular) mass/surface area (Figures 1A-H and Figures S1A-B), exercise intolerance with reduced running distance and workload (Figure 1I and Figure S1C-D), and metabolic

remodeling, including increased body fat accumulation, plasma cholesterol, glucose, and insulin levels, and HOMA-IR (Figures 1J-Q). Female mice also developed heart failure phenotypes that recapitulate clinical symptoms of HFpEF, including include diastolic dysfunction, cardiac hypertrophy, lung congestion, LV mass, LV mass/surface area and metabolic remodeling (Figures S2A-S).

We also developed the HFpEF model in 30 genetically diverse inbred strains of male and female mice, a subset of Hybrid Mouse Diversity Panel (HMDP), to examine trait-trait correlations across genetic perturbations. In both sexes, the metabolic traits glucose tolerance, HOMA-IR, plasma cholesterol levels and insulin levels were positively correlated with the diastolic parameters E/e' ratio and E/A ratio (Figures 1R-U and Figures S3A-D). These results reveal a clear metabolic remodeling induced by the HFpEF diet and a positive association between metabolic and diastolic dysfunction.

Reduced systemic IPA levels in mice with HFpEF

We performed metabolomics of heart tissue and plasma from C57BL/6J male and female mice after 7 weeks of chow diet or HFD + l-NAME feeding to determine the metabolic signatures of HFpEF. PCA plots revealed distinct clusters of samples from chow and HFpEF mice (Figure 2A). The intermediates in the main metabolic pathways, including glycolysis, tricarboxylic acid (TCA) cycle, ketone bodies, and amino acid metabolism, were significantly differentiated in heart tissue and plasma samples from HFpEF mice relative to control mice (Figures 2B-C and Figures S4A-D). Notably, HFpEF mice showed a decrease of the metabolites involved in tryptophan metabolism in both male and female mice (Figures 2B-D and Figures S4A-B). In male HFpEF mice, indole-3-propionic acid (IPA) was decreased by 4.7-fold and 3.8-fold in the heart tissue and circulation, respectively (Figures 2E-F). Moreover, plasma and cardiac IPA levels in the mice were inversely correlated with E/A ratio and E/e' ratio but not with LVEF (Figures 2G-I). Female mice fed with HFD + l-NAME exhibited similar metabolic changes relative to controls (Figures S4A-B), and IPA was consistently decreased in the plasma and heart tissue (Figures S4C-D). IPA levels were also significantly decreased in the liver and the white adipose tissue (WAT) in the mice fed with HFD + l-NAME relative to controls (Figures S5A-B), indicating a systemic response to HFpEF.

IPA attenuates diastolic and metabolic dysfunction in HFpEF model

We next sought to test the effect of IPA on HFpEF. C57BL/6J male mice were fed with chow diet or HFD + l-NAME containing control or high IPA for 7 weeks (Figure 3A). Compared with control HFpEF mice, IPA-fed mice exhibited about a 20-fold increase of IPA levels in both plasma and heart tissue and about 4-fold increase compared to mice fed a chow diet (Figures 3B-C). 7 weeks of HFD + l-NAME feeding induced an increase of body weight and fat mass while IPA supplementation decreased body weight gain and body fat accumulation (Figures 3D-E) [27]. IPA supplementation attenuated glucose intolerance and insulin resistance in HFpEF mice (Figures 3F-G). In addition, IPA reduced white and brown adipose tissue (BAT) mass without affecting lean body mass (Figures 3H-I and Figure S6A), indicating improved body composition. Food intake was not changed by IPA feeding (Figure S6B), indicating no difference in caloric intake. Consistent with improved

glucose metabolism, IPA improved lipid homeostasis as assessed by reduced cholesterol and free fatty acids in both the circulation and the heart (Figures 3J-L and Figures S6C-D). Importantly, mice fed with IPA exhibited improved diastolic function as assessed by heart weight, E/A ratio, E/e' ratio, LV mass/surface area, lung congestion and exercise tolerance (Figures 3M-R and Figures S6E-L). In contrast, LVEF was unchanged by IPA or HFD + l-NAME (Figure S6F), highlighting the specificity of the models to HFpEF. IPA significantly mitigated hypertrophy and fibrosis of the heart tissue induced by HFpEF (Figures S6M-O).

The epithelial layer of cells isolated from the small intestine of mice fed on HFD + l-NAME containing either control or high IPA were analyzed using 10x Genomics Chromium droplet single cell RNA sequencing (scRNA-seq). We examined the transporters for key nutrient families (fat and cholesterol, amino acid, peptide, and carbohydrate) in each cell of enterocyte cluster. Modulated signature scores indicate that expression of the carbohydrate transporters and the peptide transporters decreased in the high IPA feeding group (Figures S7A-F). Further assessment indicated that expression of UCP1 and NDUFS1 increased slightly in the BAT of mice fed with high IPA diet (Figures S8A-B). However, the core body temperature between control and high IPA feeding mice remained the same (Figure S8C). Multiple factors might contribute to the body temperature regulation, and the upregulation of NDUFS1 and UCP1 in BAT might not be sufficient to solely increase body temperature differences [28]. The differences in body weight gain and BAT weight also became less significant at 30 °C thermoneutral housing temperatures (Figure S8D-F).

Furthermore, we tested the impact of IPA on diastolic function in C57BL/6J female mice (Figure S9A). Consistent with the phenotypes observed in male mice, female mice fed with IPA displayed reduced body weight gain and reduced fat mass gain when subjected to the HFpEF diet (Figures S9B-D). Also, IPA improved diastolic dysfunction in HFpEF mice, as assessed by reduced E/A ratio, E/e' ratio, LV mass, heart weight, and lung weight (Figures S9E-J). Moreover, total adipose mass and plasma cholesterol were also reduced (Figures S9K-N). Thus, IPA protected against diastolic and metabolic dysfunction in the HFpEF mouse model.

IPA mitigates gut microbiota dysbiosis and intestinal epithelial barrier damage

IPA has been reported to protect against the gut microbiota dysbiosis and intestinal epithelial barrier damage induced by a high-fat diet [29]. We therefore examined the gut microbiota and intestinal epithelium in the mice fed with chow diet, HFD + l-NAME or HFD + l-NAME containing high IPA for 7 weeks. Ceca were collected and 16S rRNA-based gut microbial profiling was performed. HFpEF mice exhibited substantial gut microbiota dysbiosis including a decrease of *Bacteroidetes* and an increase of *Firmicutes*/*Bacteroidetes* ratios (Figures S10A-D) [30]. IPA reduced *Firmicutes* abundance and restored *Bacteroidetes* abundance, thus reversing *Firmicutes*/*Bacteroidetes* ratio induced by HFD + l-NAME (Figures S10A-D).

In accordance with induced dysbiosis, the HFpEF model exhibited abnormal morphological alterations of small intestines including increased villus width and reduced villus length (Figures S10E-G). IPA restored villus width and length (Figures S10E-G), suggesting that IPA has a beneficial effect on epithelial homeostasis. Furthermore, we examined the

expression of occludin, a tight junction protein in the epithelium, by immunostaining and immunoblotting. Compared with normal controls, occludin was decreased in the intestines of HFpEF mice, and IPA supplementation significantly upregulated occludin expression (Figures S10H-K). Together, these results demonstrate that IPA protects against gut microbiota dysbiosis and intestinal epithelial barrier damage in HFpEF mice. We note that IPA is known to be produced from tryptophan by *Clostridium sporogenes*, which does not belong to either the *Firmicutes* or *Bacteroidetes* phyla [11].

IPA restores SIRT3 and the NAD salvage pathway in the heart of HFpEF mice

We next sought to examine the metabolic effect of IPA supplementation in HFpEF mice. IPA reduced branched-chain amino acids, riboflavin, and tryptophan in the heart (Figures 4A-B). In contrast, IPA augmented ketone body levels and showed a tendency to increased intermediates in the TCA cycle (Figures 4A-B and Figures S11A-B). Notably, nicotinamide (NAM) levels were decreased in the heart of HFpEF mice relative to controls. This was significantly reversed by IPA (Figure 4C) such that NAM levels were positively correlated with IPA levels in the heart (Figure 4D). As a precursor of NAD^+, NAM has been shown to have substantive beneficial effects on cardiometabolic diseases by mediating NAD bioavailability (Figure 4E) [26, 31]. Consistent with the level of NAM, we observed reduced NAD^+/NADH level in the heart of HFpEF mice, and IPA restored the NAD^+/NADH level (Figure 4F). In addition, IPA significantly reduced plasma lipopolysaccharide (LPS) levels, inflammatory gene expression and oxidative stress in the heart (Figures 4G-H and Figures S11C-D). We conducted new experiments and examined mitochondrial activity in HFpEF mice. The results indicate that IPA intervention tends to increase overall mitochondrial activity in the heart in mice (Figures S11E-J), which could contribute to the improved diastolic dysfunction. Moreover, the sum of two forms of NAD indicates that the global pool of NAD decreased in the heart of HFpEF mice (Figures S12A-C), and IPA supplementation increased the total NAD (Figures S12D-F).

We then examined the key mediators involved in the NAD-NAM circuit. IPA supplementation increased the expression of Sirtuin 3 (SIRT3) and decreased nicotinamide N-methyltransferase (NNMT) in the heart (Figures 4I-J and Figures S12G-H), normalizing regulation of NAD-NAM circuit in the heart. In accordance with NNMT protein, NNMT activity was decreased by IPA in the heart tissue of HFpEF (Figures S12I-J). In accordance with SIRT3 protein, lysine acetylation was increased in the heart tissue of HFpEF mice, and IPA decreased acetylation (Figure S12K) [32].

We performed a careful assessment of the methyl-NAM and its downstream metabolites to achieve a fuller characterization of NAD^+ metabolome. The results showed that methyl-NAM increased in the heart of HFpEF mice (Figure S13A). IPA supplementation decreased the methyl-NAM abundance in the heart, as well as in the liver and plasma (Figures S13B-D). The abundance of its downstream metabolites 2-PY/4-PY also decreased in the heart, liver, plasma and urine (Figures S13E-H) of mice fed with a high-IPA diet, in accordance with the decrease of NNMT and methyl-NAM in mice fed with a high-IPA diet.

To analyze this pathway more thoroughly and achieve a broader understanding of the impact of IPA on NAD metabolism, we examined the expression of key genes involved in NAD

synthesis and NAD hydrolysis. Several key genes involved in NAD synthesis, including *Nmrk2*, *Nmnat1* and *Nmnat2*, were increased in the heart of mice fed with high-IPA diet (Figure S13I). The expression levels of *Nampt* and *Nmnat2* were increased by IPA in the liver (Figure S13J). We also examined the genes involved in NAD hydrolysis. The results indicated that the expression *Parp1* was increased by IPA in all organs examined, including the heart, liver and WAT (Figures S13I-K). The expression of *Cd38* was also increased in the liver upon IPA feeding (Figure S13J). These results show that IPA increases the total NAD pool and increases the expression of genes involved in both NAD synthesis and NAD hydrolysis at the same time.

We also assessed the expression of SIRT3 and NNMT in the liver and the WAT. The results indicate that the NNMT levels in both the liver and WAT dramatically increased in the HFpEF mice compared with control mice and were decreased by IPA supplementation (Figures S14A-F). The SIRT3 levels were decreased in the liver and WAT of HFpEF mice and were upregulated by IPA supplementation (Figures S14A-F). Overall, these results indicate IPA has a significant impact on the NAD metabolism and that these biological effects of IPA are systemic.

IPA promotes SIRT3 expression through the ligand binding of AhR in the heart

Two IPA receptors have been previously reported: the pregnane X receptor (PXR) and the aryl hydrocarbon receptor (AhR) [16, 17, 33–35]. We found that only AhR was present in the heart as PXR was not detected. We also found that IPA treatment increased AhR levels (Figures S15A-B) and some upstream regulators of AhR transcription increased upon IPA treatment (Figure S15C).

In the classical mechanism of AhR activation as a transcription factor, ligand binding stimulates AhR nuclear translocation and dimerization with other proteins, resulting in the formation of unique protein complexes that bind to their DNA binding sites and stimulate gene expression [16, 17, 33–35]. To investigate whether IPA binding could promote AhR nuclear translocation, we assessed AhR protein levels in the nuclear and cytosolic compartments, respectively, in HL-1 cells treated with control or IPA in the presence of phenylephrine (PE) (Figure S15D). AhR protein levels were dramatically increased in the nucleus and decreased in the cytosol (Figures S15E-F). To examine the activation status of AhR, we examined several well defined AhR target genes of the CYP1A1 and CYP1B family. The results show that both the expression of *Cyp1a1* and *Cyp1b1* significantly increased in the heart of mice fed with high-IPA diet compared with the controls (Figures S15G-I). Similar levels of activation were observed in the liver and WAT (Figures S15J-Q). These results indicate that the high-IPA feeding group exhibits increased AhR activation status.

We further examined whether AhR promotes SIRT3 expression as a transcription factor. We inhibited the AhR using its antagonist CH-223191 to test if it mediates the molecular regulation of IPA on cardiomyocytes[17] (Figures 4K-M and Figures S16A-C). A total of 6 groups, including control, control with IPA only, PE, PE with IPA only, PE with CH inhibitor, and PE with CH inhibitor plus IPA, were included in this study, and both protein levels and mRNA levels were examined. The results indicate that CH-223191 suppressed the upregulation of SIRT3 by IPA treatment, confirming that IPA promotes SIRT3 expression

through its binding with AhR and subsequently nuclear translocation (Figures 4K-M and Figures S16A-C). Moreover, we identified putative AhR binding sites within the *Sirt3* promoter region (TGCGTG) [36]. Subsequently, we conducted a ChIP assay to test the interaction between AhR protein and the *Sirt3* promoter. Our results indicate that AhR binds to promoter region of *Sirt3* (Figure S16D). Collectively, these results demonstrate that IPA regulates *Sirt3* through AhR.

In regard to the downregulation of cardiac NNMT by IPA, it has been reported that the proinflammatory cytokines, such as IL-6 and TNF-a, elicit significant induction of NNMT expression [37]. Since IPA has whole-body anti-inflammatory effects in multiple disease models [23, 29, 38, 39], we examined whether IPA could downregulate cardiac NNMT through an anti-inflammatory response. The expression of proinflammatory cytokine TNF-α is increased in the mice heart upon HFpEF diet feeding and IPA supplementation decreased TNF-α expression, in accordance with the expression of NNMT (Figures 4I-J). Also, IPA treatment in vitro of cardiomyocytes alone did not significantly decrease the NNMT levels (Figures 4K-M). To determine whether proinflammatory cytokines could promote the expression of NNMT, we examined NNMT expression in HL-1 cells incubated with different concentrations of TNF-a in the presence of PE. The results show that TNF-a does induce the expression of NNMT in cardiomyocytes (Figures S16E-F). Furthermore, we also examined whether IPA has a comprehensive impact on proinflammatory cytokines in HFpEF mice. The results indicate that IPA suppresses the expression of proinflammatory cytokines in the mice heart, such as TNF-a, IL-6 and IL-1β (Figure S16G). These results demonstrate that IPA at least partially decreases the cardiac NNMT through the inhibition of proinflammatory cytokine expression.

We conducted experiments using AhR siRNA knockdown to study the impact of IPA stimulation. The results showed that AhR knockdown suppressed the upregulation of SIRT3 by IPA treatment, indicating that IPA promotes SIRT3 expression through its binding with AhR (Figures S17A-C). We also performed RT-qPCR analysis in all these 6 groups, and the mRNA expression levels were in accordance with the protein levels (Figures S17D-F). Furthermore, to test if SIRT3 mediates the effects of IPA in vivo, we knocked down mRNA encoding SIRT3 in the hearts of C57BL/6J male mice using AAV9 delivery of shRNA (Figures 4N-P). *Sirt3* knockdown diminished the effects of IPA on body mass and diastolic dysfunction in the HFpEF model (Figures 4Q-W), suggesting that SIRT3 plays a critical role in the protective effects of IPA on diastolic dysfunction.

Nicotinamide (NAM) mitigates diastolic dysfunction in HFpEF

NAM was reported to protect against diastolic dysfunction in the models of obesity and HFpEF [26]. We thus fed C57BL/6J male mice with NAM to assess its effect on heart function. NAM feeding significantly increased heart NAM and NAD^+ levels (Figures 5A-B). The results indicate that NAM supplementation dramatically increased levels of methyl-NAM and its downstream metabolites 2-PY/4-PY in the plasma, liver, heart and urine (Figures S18A-G). Surprisingly, NAM feeding reversed the *Bacteroidetes* and *Firmicutes/Bacteroidetes* ratio induced by HFpEF, in common with IPA feeding (Figures 5C-F). The mice receiving NAM exhibited reduced body weight gain and fat accumulation with

comparable food intake relative to controls in the progression to HFpEF (Figures 5G-I and Figure S19A). Accordingly, NAM improved glucose tolerance and plasma free fatty acids (Figures 5J-K). Consistent with these results, mice receiving NAM exhibited attenuated diastolic dysfunction and cardiac hypertrophy as assessed by mitigated E/A ratio, E/e' ratio, LV mass/surface area, lung congestion and improved exercise tolerance (Figures 5L-Q and Figures S19B-G). Further, we fed mice with the combination of IPA and NAM, together with HFD + l-NAME. The combination of IPA and NAM mitigated diastolic dysfunction and metabolic disorders to a similar extent as IPA or NAM treatment alone, suggesting they target the same pathway affecting diastolic function, although this does not eliminate the possibility that other pathways are involved (Fig. 5R-X). Furthermore, HFD + l-NAME feeding increased the systolic BP and diastolic BP in the mice, and high-NAM supplementation decreased systolic BP in mice, comparable with high-IPA supplementation (Figures S19H-I).

Nnmt knockdown mitigates diastolic dysfunction in HFpEF

To further test if reducing NAM breakdown protects against diastolic dysfunction in HFpEF, we knocked down mRNA encoding nicotinamide N-methyltransferase (NNMT), the enzyme that catalyzes the N-methylation of NAM, with an antisense oligonucleotide (ASO) [40]. *Nnmt* ASO or control ASO were injected weekly into C57BL/6J male mice maintained on HFD + l-NAME for 7 weeks. *Nnmt* ASO dramatically decreased heart NNMT expression (Figure 6A and Figure S20A). Consistently, mice receiving *Nnmt* ASO exhibited decreased body weight gain and fat mass accumulation with no changes in lean mass or food intake relative to those receiving control ASO (Figures 6B-D and Figure S20B). The *Nnmt* ASO improved glucose homeostasis and insulin resistance, in common with IPA feeding (Figures 6E-F). In addition, plasma insulin, HOMA-IR, plasma triglycerides, total cholesterol, and unesterified cholesterol were consistently decreased in the mice receiving the *Nnmt* ASO (Figures 6G-K). Consistent with the effects of NAM feeding, the *Nnmt* ASO significantly improved diastolic function as measured by improved exercise tolerance, reduced E/A ratio, E/e' ratio, LV mass/surface area and lung congestion compared with control ASO (Figures 6L-Q and Figures S20C-H). These results collectively demonstrate the protective effect of *Nnmt* knockdown in the HFpEF mouse model.

Additionally, we overexpressed *Nnmt* in the model of HFpEF to test if it mediates the effects of IPA on diastolic function. *Nnmt* overexpression using AAV9-cTnT-*Nnmt* dramatically increased heart NNMT expression (Figure 6R and Figure S20I). *Nnmt* overexpression in the heart diminished the effects of IPA on body mass and diastolic dysfunction in HFpEF (Figures 6S-Y), demonstrating that IPA protects against diastolic dysfunction through the NAD-NAM circuit.

Therapeutic effects of IPA in HFpEF

To test if IPA is beneficial after diastolic dysfunction has developed, we fed C57BL/6J male mice with chow diet or HFD + l-NAME to induce HFpEF phenotypes, followed by IPA supplementation (Figure 7A). 4 weeks of HFD + l-NAME induced HFpEF phenotypes as confirmed by increased body weight, plasma cholesterol, E/A ratio and E/e' ratio (Figures 1 and Figures 7B-K). The mice fed with HFD + l-NAME diet were then fed with HFD +

l-NAME containing control or high IPA for another 5 weeks. Mice fed with IPA exhibited significantly lower body weight, adipose tissue weight, and metabolic remodeling compared with the mice from control group (Figures 7B-H). In addition, IPA significantly blunted the progression of diastolic dysfunction, as measured by lower E/A ratio, E/e' ratio, heart weight, LV mass/surface area, preserved LVEF, lung congestion, and increased exercise tolerance (Figures 7I-Q and Figures S21A-C). These observations support the therapeutic effect of IPA in the HFpEF model.

IPA levels are reduced in HFpEF patients

To determine the clinical relevance of IPA, we quantified plasma IPA levels in Cleveland Clinic participants without heart failure (n = 48) and ambulatory patients with chronic HFpEF (n = 48) using LC-MS/MS analysis. Chronic HFpEF subjects were clinically diagnosed with HF for at least 6 months prior to enrollment with a left ventricular ejection fraction (LVEF) ≥ 50% (characterized in Table S1). In this human HFpEF cohort with matched age and sex, IPA levels were significantly reduced in HFpEF patients compared with non-heart failure controls (Figure 8A and Table S1). Elevated IPA levels were inversely associated with HFpEF independent of age, sex, diabetes, and hypercholesterolemia [4th quartile, unadjusted odds ratio (OR) 0.30, 95% confidence interval (CI) 0.088–0.96, P<0.05; adjusted OR (model 1) 0.28, 95% CI 0.078–0.92, P<0.05]. When BMI and hypertension were included in the multivariable logistic regression model (adjusted model 2), the inverse association between IPA levels and HFpEF was attenuated [adjusted OR (model 2) 0.33, 95% CI 0.085–1.16, P=0.09] (Figure 8B and Table S2). When IPA was treated as a continuous variable in the logistic regression models, similar results were observed [OR for HFpEF per interquartile range (IQR) increase of IPA, unadjusted OR 0.41, 95% CI 0.16–0.93, P<0.05; adjusted OR (model 1) 0.39, 95% CI 0.15–0.90, P<0.05; adjusted OR (model 2) 0.48, 95% CI 0.18–1.18, P=0.13] (Table S2).

In a separate human cohort from Alfred Hospital at Melbourne, HFpEF patients (n = 22) were collected for investigation of symptoms consistent with a diagnosis of heart failure (NYHA II-III) in the presence of a LVEF > 50%, and a HFrEF cohort (n = 20) had LVEF < 40% (Figure 8C and Table S3**)**. The diagnosis of HFpEF was confirmed by the presence of an end-expiratory pulmonary capillary wedge pressure (PCWP) ≥ 15 mmHg at rest or ≥ 25 mmHg during symptom-limited exercise. In this cohort, arterial IPA abundance was significantly decreased in HFpEF patients relative to non-HF controls (Figure 8D). There results collectively reveal a significant reduction of IPA in HFpEF patients, consistent with our results in the mouse model.

Discussion

HFpEF accounts for half of all heart failure worldwide, conferring substantial morbidity and mortality. Compared to patients with HFrEF, patients with HFpEF display a metabolic profile characterized by insulin resistance, inflammation, oxidative stress, and impaired lipid metabolism [41]. Using the HFpEF mouse model, we examined both males and females of 30 diverse inbred strains of mice, a subset of the Hybrid Mouse Diversity Panel (HMDP), confirming the association between diastolic and metabolic dysfunction.

Tryptophan metabolism was reduced in HFpEF mice and IPA levels were decreased in the heart and circulation. IPA supplementation protected against diastolic dysfunction in the progression of HFpEF and in therapeutic management after the development of HFpEF phenotypes. Mechanistically, IPA exerts both direct and indirect impacts on the heart. Specifically, we found that IPA enhances intestinal barrier function, reduces body weight and promotes glucose and lipid homeostasis. In the context of the heart, IPA directly restored the NAD salvage pathway through activation of the AhR and expression of SIRT3, thereby improving metabolic and diastolic dysfunction associated with HFpEF. To determine whether our findings in the HFpEF model are relevant to humans, we examined two separate cohorts of heart failure patients with HFpEF. Indeed, in both cohorts, the levels of IPA were significantly reduced in HFpEF patients, suggesting that IPA levels exert a major impact on the disease (Figure 8E). Moreover, IPA has previously been reported to ameliorate inflammation and cell oxidative damage [11, 24, 42]. Elevated concentrations of IPA in human blood plasma were correlated with a lower risk of type 2 diabetes [23, 24] and reduced proportions of IPA-producing bacteria were found in patients with type 2 diabetes [43, 44]. In other studies, IPA has been reported to show neuroprotective, antioxidant, antitubercular, and anti-amyloid properties, to modulate mitochondrial function, and to protect against radiation toxicity [21, 45–47].

Our data indicate that IPA appears to be acting in the heart by at least two pathways. One of these is mediated by AhR binding and subsequently nuclear translocation to activate the SIRT3 expression. On the other hand, NNMT suppression by IPA appears to be secondary to suppression of inflammation. The evidence indicating the involvement of the NAD salvage pathway (from NAM to NMN to NAD) is strong. Prior to our studies, the Hill laboratory reported using the “two-hit” model that NMN supplementation improved diastolic function and related parameters in HFpEF [25]. Our results, showing that IPA suppresses NNMT, increasing NAM levels and increasing NAD salvage, is entirely consistent with this. Notably, inhibition of NNMT by an antisense oligonucleotide increased NAM levels and improved diastolic function. In our study, administration of IPA restored heart NAM, NAD^+/NADH levels and the expression of SIRT3. SIRT3 has previously been shown to be modulated by NAD availability and exhibit protective effects in aging, diabetes, obesity, hypertension and heart failure [48–53]. The fact that treatment of HFpEF mice with IPA or NAM, or the combination of IPA and NAM, all reduced diastolic function to about the same extent suggests a common pathway of action. Consistent with our conclusions, nicotinamide has recently been shown to protect against diastolic dysfunction, glaucoma, and hepatic steatosis by mediating NAD bioavailability, mitochondrial function, oxidative stress, inflammation and protein deacetylation [26, 31]. NNMT was found to be increased in HFD-fed mice [40, 54]. In addition, NNMT overexpression decreased the NAD^+ content in the liver and promoted liver steatosis and fibrosis [55].

There may be other potential pathways involved in the attenuation of diastolic dysfunction by IPA. For example, IPA supplementation in HFpEF mice involved augmented ketone body levels and a tendency to increased intermediates in the TCA cycle. Ketone bodies and TCA cycle play important roles in energy metabolism including ATP production of the failing heart [56–59]. The systemic beneficial effects of IPA are likely to contribute to a decrease in body weight. It has been reported that IPA supplementation improves blood glucose,

increases insulin sensitivity [60], inhibits liver lipid synthesis and inflammatory factors [18], corrects intestinal microbial disorders [29], and suppresses the intestinal immune response [61]. The extent to which the beneficial effects of IPA on HFpEF are attributable to its capacity to decrease body weight requires further investigation.

The number of human samples in our study was relatively small and it will be important to explore IPA effects in larger cohorts of HFpEF patients. While we have not examined the effects of tryptophan supplementation or perturbations of IPA-producing gut microbes, our results suggest that these may protect against HFpEF as well as other metabolic disorders. Mechanistically, IPA reduces NAM catabolism and elevates NAD^+ levels in the heart. In addition to the effects on NAM and NAD^+ levels, IPA reduced intestinal dysbiosis, which may also contribute to improved diastolic and metabolic functions in HFpEF mice. Moreover, along with previous studies showing that NAD^+ replenishment can improve symptoms of HFpEF patients [25, 26], our findings support a potential therapeutic effect of IPA on HFpEF traits.

Supplementary Material

Refer to Web version on PubMed Central for supplementary material.

Sources of Funding

This work was supported by NIH grants HL144651 and HL148577. H.A. was supported by NIH grants HL133169 and HL148110. S.L.H. was supported by NIH grant R01HL167831 and P01HL147823.

Non-standard Abbreviations and Acronyms

AAV	adeno-associated virus
AhR	aryl hydrocarbon receptor
ASO	antisense oligonucleotides
BAT	brown adipose tissue
HFD	high-fat diet
HFpEF	heart failure with preserved ejection fraction
HMDP	hybrid mouse diversity panel
IPA	indole-3-propionic acid
LC-MS	liquid chromatography–mass spectrometry
l-NAME	Nω-Nitro-L-arginine methyl ester hydrochloride
LVEF	left ventricular ejection fraction
NAD	nicotinamide adenine dinucleotide
NAM	nicotinamide

NDUFS1	NADH:ubiquinone oxidoreductase core subunit S1
NMR	nuclear magnetic resonance
NNMT	nicotinamide N-methyltransferase
OR	odds ratio
PE	phenylephrine
SIRT	sirtuin
UCP1	uncoupling protein 1
WAT	white adipose tissue

References

1. Dunlay SM, Roger VL and Redfield MM. Epidemiology of heart failure with preserved ejection fraction. Nat Rev Cardiol 2017;14:591–602. [PubMed: 28492288]
2. Iwano H and Little WC. Heart failure: what does ejection fraction have to do with it? J Cardiol 2013;62:1–3. [PubMed: 23672790]
3. Zheng SL, Chan FT, Nabeebaccus AA, Shah AM, McDonagh T, Okonko DO and Ayis S. Drug treatment effects on outcomes in heart failure with preserved ejection fraction: a systematic review and meta-analysis. Heart 2018;104:407–415. [PubMed: 28780577]
4. Owan TE, Hodge DO, Herges RM, Jacobsen SJ, Roger VL and Redfield MM. Trends in prevalence and outcome of heart failure with preserved ejection fraction. N Engl J Med 2006;355:251–9. [PubMed: 16855265]
5. Lam CS, Donal E, Kraigher-Krainer E and Vasan RS. Epidemiology and clinical course of heart failure with preserved ejection fraction. Eur J Heart Fail 2011;13:18–28. [PubMed: 20685685]
6. Cheng RK, Cox M, Neely ML, Heidenreich PA, Bhatt DL, Eapen ZJ, Hernandez AF, Butler J, Yancy CW and Fonarow GC. Outcomes in patients with heart failure with preserved, borderline, and reduced ejection fraction in the Medicare population. Am Heart J 2014;168:721–30. [PubMed: 25440801]
7. Nassif ME, Windsor SL, Borlaug BA, Kitzman DW, Shah SJ, Tang F, Khariton Y, Malik AO, Khumri T, Umpierrez G, Lamba S, Sharma K, Khan SS, Chandra L, Gordon RA, Ryan JJ, Chaudhry SP, Joseph SM, Chow CH, Kanwar MK, Pursley M, Siraj ES, Lewis GD, Clemson BS, Fong M and Kosiborod MN. The SGLT2 inhibitor dapagliflozin in heart failure with preserved ejection fraction: a multicenter randomized trial. Nat Med 2021;27:1954–1960. [PubMed: 34711976]
8. Hogg K, Swedberg K and McMurray J. Heart failure with preserved left ventricular systolic function; epidemiology, clinical characteristics, and prognosis. J Am Coll Cardiol 2004;43:317–27. [PubMed: 15013109]
9. Mishra S and Kass DA. Cellular and molecular pathobiology of heart failure with preserved ejection fraction. Nat Rev Cardiol 2021;18:400–423. [PubMed: 33432192]
10. Schiattarella GG, Altamirano F, Tong D, French KM, Villalobos E, Kim SY, Luo X, Jiang N, May HI, Wang ZV, Hill TM, Mammen PPA, Huang J, Lee DI, Hahn VS, Sharma K, Kass DA, Lavandero S, Gillette TG and Hill JA. Nitrosative stress drives heart failure with preserved ejection fraction. Nature 2019;568:351–356. [PubMed: 30971818]
11. Wikoff WR, Anfora AT, Liu J, Schultz PG, Lesley SA, Peters EC and Siuzdak G. Metabolomics analysis reveals large effects of gut microflora on mammalian blood metabolites. Proc Natl Acad Sci U S A 2009;106:3698–703. [PubMed: 19234110]
12. Attwood G, Li D, Pacheco D and Tavendale M. Production of indolic compounds by rumen bacteria isolated from grazing ruminants. J Appl Microbiol 2006;100:1261–71. [PubMed: 16696673]

13. Liu Y, Chen H, Van Treuren W, Hou BH, Higginbottom SK and Dodd D. Clostridium sporogenes uses reductive Stickland metabolism in the gut to generate ATP and produce circulating metabolites. Nat Microbiol 2022;7:695–706. [PubMed: 35505245]

14. Kaluzna-Czaplinska J, Gatarek P, Chirumbolo S, Chartrand MS and Bjorklund G. How important is tryptophan in human health? Crit Rev Food Sci Nutr 2019;59:72–88. [PubMed: 28799778]

15. Cao Y, Aquino-Martinez R, Hutchison E, Allayee H, Lusis AJ and Rey FE. Role of gut microbe-derived metabolites in cardiometabolic diseases: Systems based approach. Mol Metab 2022;64:101557. [PubMed: 35870705]

16. Zhang LS and Davies SS. Microbial metabolism of dietary components to bioactive metabolites: opportunities for new therapeutic interventions. Genome Med 2016;8:46. [PubMed: 27102537]

17. Rothhammer V, Mascanfroni ID, Bunse L, Takenaka MC, Kenison JE, Mayo L, Chao CC, Patel B, Yan R, Blain M, Alvarez JI, Kebir H, Anandasabapathy N, Izquierdo G, Jung S, Obholzer N, Pochet N, Clish CB, Prinz M, Prat A, Antel J and Quintana FJ. Type I interferons and microbial metabolites of tryptophan modulate astrocyte activity and central nervous system inflammation via the aryl hydrocarbon receptor. Nat Med 2016;22:586–97. [PubMed: 27158906]

18. Li Y, Xu W, Zhang F, Zhong S, Sun Y, Huo J, Zhu J and Wu C. The Gut Microbiota-Produced Indole-3-Propionic Acid Confers the Antihyperlipidemic Effect of Mulberry-Derived 1-Deoxynojirimycin. mSystems 2020;5.

19. Dodd D, Spitzer MH, Van Treuren W, Merrill BD, Hryckowian AJ, Higginbottom SK, Le A, Cowan TM, Nolan GP, Fischbach MA and Sonnenburg JL. A gut bacterial pathway metabolizes aromatic amino acids into nine circulating metabolites. Nature 2017;551:648–652. [PubMed: 29168502]

20. Venkatesh M, Mukherjee S, Wang H, Li H, Sun K, Benechet AP, Qiu Z, Maher L, Redinbo MR, Phillips RS, Fleet JC, Kortagere S, Mukherjee P, Fasano A, Le Ven J, Nicholson JK, Dumas ME, Khanna KM and Mani S. Symbiotic bacterial metabolites regulate gastrointestinal barrier function via the xenobiotic sensor PXR and Toll-like receptor 4. Immunity 2014;41:296–310. [PubMed: 25065623]

21. Gesper M, Nonnast ABH, Kumowski N, Stoehr R, Schuett K, Marx N and Kappel BA. Gut-Derived Metabolite Indole-3-Propionic Acid Modulates Mitochondrial Function in Cardiomyocytes and Alters Cardiac Function. Front Med (Lausanne) 2021;8:648259. [PubMed: 33829028]

22. Konopelski P, Chabowski D, Aleksandrowicz M, Kozniewska E, Podsadni P, Szczepanska A and Ufnal M. Indole-3-propionic acid, a tryptophan-derived bacterial metabolite, increases blood pressure via cardiac and vascular mechanisms in rats. Am J Physiol Regul Integr Comp Physiol 2021;321:R969–R981. [PubMed: 34755563]

23. Tuomainen M, Lindstrom J, Lehtonen M, Auriola S, Pihlajamaki J, Peltonen M, Tuomilehto J, Uusitupa M, de Mello VD and Hanhineva K. Associations of serum indolepropionic acid, a gut microbiota metabolite, with type 2 diabetes and low-grade inflammation in high-risk individuals. Nutr Diabetes 2018;8:35. [PubMed: 29795366]

24. de Mello VD, Paananen J, Lindstrom J, Lankinen MA, Shi L, Kuusisto J, Pihlajamaki J, Auriola S, Lehtonen M, Rolandsson O, Bergdahl IA, Nordin E, Ilanne-Parikka P, Keinanen-Kiukaanniemi S, Landberg R, Eriksson JG, Tuomilehto J, Hanhineva K and Uusitupa M. Indolepropionic acid and novel lipid metabolites are associated with a lower risk of type 2 diabetes in the Finnish Diabetes Prevention Study. Sci Rep 2017;7:46337. [PubMed: 28397877]

25. Tong D, Schiattarella GG, Jiang N, Altamirano F, Szweda PA, Elnwasany A, Lee DI, Yoo H, Kass DA, Szweda LI, Lavandero S, Verdin E, Gillette TG and Hill JA. NAD(+) Repletion Reverses Heart Failure With Preserved Ejection Fraction. Circ Res 2021;128:1629–1641. [PubMed: 33882692]

26. Abdellatif M, Trummer-Herbst V, Koser F, Durand S, Adao R, Vasques-Novoa F, Freundt JK, Voglhuber J, Pricolo MR, Kasa M, Turk C, Aprahamian F, Herrero-Galan E, Hofer SJ, Pendl T, Rech L, Kargl J, Anto-Michel N, Ljubojevic-Holzer S, Schipke J, Brandenberger C, Auer M, Schreiber R, Koyani CN, Heinemann A, Zirlik A, Schmidt A, von Lewinski D, Scherr D, Rainer PP, von Maltzahn J, Muhlfeld C, Kruger M, Frank S, Madeo F, Eisenberg T, Prokesch A, Leite-Moreira AF, Lourenco AP, Alegre-Cebollada J, Kiechl S, Linke WA, Kroemer G and Sedej

S. Nicotinamide for the treatment of heart failure with preserved ejection fraction. Sci Transl Med 2021;13.

27. Konopelski P, Konop M, Gawrys-Kopczynska M, Podsadni P, Szczepanska A and Ufnal M. Indole-3-Propionic Acid, a Tryptophan-Derived Bacterial Metabolite, Reduces Weight Gain in Rats. Nutrients 2019;11.
28. Keipert S, Lutter D, Schroeder BO, Brandt D, Stahlman M, Schwarzmayr T, Graf E, Fuchs H, de Angelis MH, Tschop MH, Rozman J and Jastroch M. Endogenous FGF21-signaling controls paradoxical obesity resistance of UCP1-deficient mice. Nat Commun 2020;11:624. [PubMed: 32005798]
29. Zhao ZH, Xin FZ, Xue Y, Hu Z, Han Y, Ma F, Zhou D, Liu XL, Cui A, Liu Z, Liu Y, Gao J, Pan Q, Li Y and Fan JG. Indole-3-propionic acid inhibits gut dysbiosis and endotoxin leakage to attenuate steatohepatitis in rats. Exp Mol Med 2019;51:1–14.
30. Turnbaugh PJ, Ley RE, Mahowald MA, Magrini V, Mardis ER and Gordon JI. An obesity-associated gut microbiome with increased capacity for energy harvest. Nature 2006;444:1027–31. [PubMed: 17183312]
31. Mitchell SJ, Bernier M, Aon MA, Cortassa S, Kim EY, Fang EF, Palacios HH, Ali A, Navas-Enamorado I, Di Francesco A, Kaiser TA, Waltz TB, Zhang N, Ellis JL, Elliott PJ, Frederick DW, Bohr VA, Schmidt MS, Brenner C, Sinclair DA, Sauve AA, Baur JA and de Cabo R. Nicotinamide Improves Aspects of Healthspan, but Not Lifespan, in Mice. Cell Metab 2018;27:667–676 e4. [PubMed: 29514072]
32. Deng Y, Xie M, Li Q, Xu X, Ou W, Zhang Y, Xiao H, Yu H, Zheng Y, Liang Y, Jiang C, Chen G, Du D, Zheng W, Wang S, Gong M, Chen Y, Tian R and Li T. Targeting Mitochondria-Inflammation Circuit by beta-Hydroxybutyrate Mitigates HFpEF. Circ Res 2021;128:232–245. [PubMed: 33176578]
33. Agus A, Planchais J and Sokol H. Gut Microbiota Regulation of Tryptophan Metabolism in Health and Disease. Cell Host Microbe 2018;23:716–724. [PubMed: 29902437]
34. Hubbard TD, Murray IA and Perdew GH. Indole and Tryptophan Metabolism: Endogenous and Dietary Routes to Ah Receptor Activation. Drug Metab Dispos 2015;43:1522–35. [PubMed: 26041783]
35. Zelante T, Iannitti RG, Cunha C, De Luca A, Giovannini G, Pieraccini G, Zecchi R, D'Angelo C, Massi-Benedetti C, Fallarino F, Carvalho A, Puccetti P and Romani L. Tryptophan catabolites from microbiota engage aryl hydrocarbon receptor and balance mucosal reactivity via interleukin-22. Immunity 2013;39:372–85. [PubMed: 23973224]
36. DeGroot DE and Denison MS. Nucleotide specificity of DNA binding of the aryl hydrocarbon receptor:ARNT complex is unaffected by ligand structure. Toxicol Sci 2014;137:102–13. [PubMed: 24136190]
37. Kim HC, Mofarrahi M, Vassilakopoulos T, Maltais F, Sigala I, Debigare R, Bellenis I and Hussain SN. Expression and functional significance of nicotinamide N-methyl transferase in skeletal muscles of patients with chronic obstructive pulmonary disease. Am J Respir Crit Care Med 2010;181:797–805. [PubMed: 20110558]
38. Zhuang H, Ren X, Jiang F and Zhou P. Indole-3-propionic acid alleviates chondrocytes inflammation and osteoarthritis via the AhR/NF-kappaB axis. Mol Med 2023;29:17. [PubMed: 36721094]
39. Chimerel C, Emery E, Summers DK, Keyser U, Gribble FM and Reimann F. Bacterial metabolite indole modulates incretin secretion from intestinal enteroendocrine L cells. Cell Rep 2014;9:1202–8. [PubMed: 25456122]
40. Brachs S, Polack J, Brachs M, Jahn-Hofmann K, Elvert R, Pfenninger A, Barenz F, Margerie D, Mai K, Spranger J and Kannt A. Genetic Nicotinamide N-Methyltransferase (Nnmt) Deficiency in Male Mice Improves Insulin Sensitivity in Diet-Induced Obesity but Does Not Affect Glucose Tolerance. Diabetes 2019;68:527–542. [PubMed: 30552109]
41. Hage C, Lofgren L, Michopoulos F, Nilsson R, Davidsson P, Kumar C, Ekstrom M, Eriksson MJ, Lynga P, Persson B, Wallen H, Gan LM, Persson H and Linde C. Metabolomic Profile in HFpEF vs HFrEF Patients. J Card Fail 2020;26:1050–1059. [PubMed: 32750486]

42. Chyan YJ, Poeggeler B, Omar RA, Chain DG, Frangione B, Ghiso J and Pappolla MA. Potent neuroprotective properties against the Alzheimer beta-amyloid by an endogenous melatonin-related indole structure, indole-3-propionic acid. J Biol Chem 1999;274:21937–42. [PubMed: 10419516]
43. Larsen N, Vogensen FK, van den Berg FW, Nielsen DS, Andreasen AS, Pedersen BK, Al-Soud WA, Sorensen SJ, Hansen LH and Jakobsen M. Gut microbiota in human adults with type 2 diabetes differs from non-diabetic adults. PLoS One 2010;5:e9085. [PubMed: 20140211]
44. Aw W and Fukuda S. Understanding the role of the gut ecosystem in diabetes mellitus. J Diabetes Investig 2018;9:5–12.
45. Bendheim PE, Poeggeler B, Neria E, Ziv V, Pappolla MA and Chain DG. Development of indole-3-propionic acid (OXIGON) for Alzheimer's disease. J Mol Neurosci 2002;19:213–7. [PubMed: 12212784]
46. Negatu DA, Liu JJJ, Zimmerman M, Kaya F, Dartois V, Aldrich CC, Gengenbacher M and Dick T. Whole-Cell Screen of Fragment Library Identifies Gut Microbiota Metabolite Indole Propionic Acid as Antitubercular. Antimicrob Agents Chemother 2018;62.
47. Xiao HW, Cui M, Li Y, Dong JL, Zhang SQ, Zhu CC, Jiang M, Zhu T, Wang B, Wang HC and Fan SJ. Gut microbiota-derived indole 3-propionic acid protects against radiation toxicity via retaining acyl-CoA-binding protein. Microbiome 2020;8:69. [PubMed: 32434586]
48. Dittenhafer-Reed KE, Richards AL, Fan J, Smallegan MJ, Fotuhi Siahpirani A, Kemmerer ZA, Prolla TA, Roy S, Coon JJ and Denu JM. SIRT3 mediates multi-tissue coupling for metabolic fuel switching. Cell Metab 2015;21:637–46. [PubMed: 25863253]
49. Koentges C, Pfeil K, Schnick T, Wiese S, Dahlbock R, Cimolai MC, Meyer-Steenbuck M, Cenkerova K, Hoffmann MM, Jaeger C, Odening KE, Kammerer B, Hein L, Bode C and Bugger H. SIRT3 deficiency impairs mitochondrial and contractile function in the heart. Basic Res Cardiol 2015;110:36. [PubMed: 25962702]
50. Sundaresan NR, Gupta M, Kim G, Rajamohan SB, Isbatan A and Gupta MP. Sirt3 blocks the cardiac hypertrophic response by augmenting Foxo3a-dependent antioxidant defense mechanisms in mice. J Clin Invest 2009;119:2758–71. [PubMed: 19652361]
51. Lee CF, Chavez JD, Garcia-Menendez L, Choi Y, Roe ND, Chiao YA, Edgar JS, Goo YA, Goodlett DR, Bruce JE and Tian R. Normalization of NAD+ Redox Balance as a Therapy for Heart Failure. Circulation 2016;134:883–94. [PubMed: 27489254]
52. Horton JL, Martin OJ, Lai L, Riley NM, Richards AL, Vega RB, Leone TC, Pagliarini DJ, Muoio DM, Bedi KC, Jr., Margulies KB, Coon JJ and Kelly DP. Mitochondrial protein hyperacetylation in the failing heart. JCI Insight 2016;2.
53. Parodi-Rullan RM, Chapa-Dubocq XR and Javadov S. Acetylation of Mitochondrial Proteins in the Heart: The Role of SIRT3. Front Physiol 2018;9:1094. [PubMed: 30131726]
54. Kraus D, Yang Q, Kong D, Banks AS, Zhang L, Rodgers JT, Pirinen E, Pulinilkunnil TC, Gong F, Wang YC, Cen Y, Sauve AA, Asara JM, Peroni OD, Monia BP, Bhanot S, Alhonen L, Puigserver P and Kahn BB. Nicotinamide N-methyltransferase knockdown protects against diet-induced obesity. Nature 2014;508:258–62. [PubMed: 24717514]
55. Komatsu M, Kanda T, Urai H, Kurokochi A, Kitahama R, Shigaki S, Ono T, Yukioka H, Hasegawa K, Tokuyama H, Kawabe H, Wakino S and Itoh H. NNMT activation can contribute to the development of fatty liver disease by modulating the NAD (+) metabolism. Sci Rep 2018;8:8637. [PubMed: 29872122]
56. Papazafiropoulou AK, Georgopoulos MM and Katsilambros NL. Ketone bodies and the heart. Arch Med Sci Atheroscler Dis 2021;6:e209–e214. [PubMed: 36161216]
57. Bhanpuri NH, Hallberg SJ, Williams PT, McKenzie AL, Ballard KD, Campbell WW, McCarter JP, Phinney SD and Volek JS. Cardiovascular disease risk factor responses to a type 2 diabetes care model including nutritional ketosis induced by sustained carbohydrate restriction at 1 year: an open label, non-randomized, controlled study. Cardiovasc Diabetol 2018;17:56. [PubMed: 29712560]
58. Gjuladin-Hellon T, Davies IG, Penson P and Amiri Baghbadorani R. Effects of carbohydrate-restricted diets on low-density lipoprotein cholesterol levels in overweight and obese adults: a systematic review and meta-analysis. Nutr Rev 2019;77:161–180. [PubMed: 30544168]

59. Nikolajevic Starcevic J, Janic M and Sabovic M. Molecular Mechanisms Responsible for Diastolic Dysfunction in Diabetes Mellitus Patients. Int J Mol Sci 2019;20. [PubMed: 31861461]
60. Abildgaard A, Elfving B, Hokland M, Wegener G and Lund S. The microbial metabolite indole-3-propionic acid improves glucose metabolism in rats, but does not affect behaviour. Arch Physiol Biochem 2018;124:306–312. [PubMed: 29113509]
61. Hendrikx T and Schnabl B. Indoles: metabolites produced by intestinal bacteria capable of controlling liver disease manifestation. J Intern Med 2019;286:32–40. [PubMed: 30873652]
62. Reddy YNV, Obokata M, Jones AD, Lewis GD, Shah SJ, Abouezzedine OF, Fudim M, Alhanti B, Stevenson LW, Redfield MM and Borlaug BA. Characterization of the Progression From Ambulatory to Hospitalized Heart Failure With Preserved Ejection Fraction. J Card Fail 2020;26:919–928. [PubMed: 32827644]
63. Verbrugge FH, Omote K, Reddy YNV, Sorimachi H, Obokata M and Borlaug BA. Heart failure with preserved ejection fraction in patients with normal natriuretic peptide levels is associated with increased morbidity and mortality. Eur Heart J 2022;43:1941–1951. [PubMed: 35139159]
64. Nemet I, Li XS, Haghikia A, Li L, Wilcox J, Romano KA, Buffa JA, Witkowski M, Demuth I, Konig M, Steinhagen-Thiessen E, Backhed F, Fischbach MA, Tang WHW, Landmesser U and Hazen SL. Atlas of gut microbe-derived products from aromatic amino acids and risk of cardiovascular morbidity and mortality. Eur Heart J 2023;44:3085–3096. [PubMed: 37342006]
65. Koay YC, Wali JA, Luk AWS, Macia L, Cogger VC, Pulpitel TJ, Wahl D, Solon-Biet SM, Holmes A, Simpson SJ and O'Sullivan JF. Ingestion of resistant starch by mice markedly increases microbiome-derived metabolites. FASEB J 2019;33:8033–8042. [PubMed: 30925066]
66. Tong M, Jacobs JP, McHardy IH and Braun J. Sampling of intestinal microbiota and targeted amplification of bacterial 16S rRNA genes for microbial ecologic analysis. Curr Protoc Immunol 2014;107:7 41 1–7 41 11.
67. Qiu Z and Sheridan BS. Isolating Lymphocytes from the Mouse Small Intestinal Immune System. J Vis Exp 2018.
68. Lefrancois L and Lycke N. Isolation of mouse small intestinal intraepithelial lymphocytes, Peyer's patch, and lamina propria cells. Curr Protoc Immunol 2001;Chapter 3:Unit 3 19.
69. Sydora BC, Brossay L, Hagenbaugh A, Kronenberg M and Cheroutre H. TAP-independent selection of CD8+ intestinal intraepithelial lymphocytes. J Immunol 1996;156:4209–16. [PubMed: 8666789]
70. Wang YC, Cao Y, Pan C, Zhou Z, Yang L and Lusis AJ. Intestinal cell type-specific communication networks underlie homeostasis and response to Western diet. J Exp Med 2023;220.
71. Luecken MD and Theis FJ. Current best practices in single-cell RNA-seq analysis: a tutorial. Mol Syst Biol 2019;15:e8746. [PubMed: 31217225]
72. Wang YC, Wang X, Yu J, Ma F, Li Z, Zhou Y, Zeng S, Ma X, Li YR, Neal A, Huang J, To A, Clarke N, Memarzadeh S, Pellegrini M and Yang L. Targeting monoamine oxidase A-regulated tumor-associated macrophage polarization for cancer immunotherapy. Nat Commun 2021;12:3530. [PubMed: 34112755]
73. Butler A, Hoffman P, Smibert P, Papalexi E and Satija R. Integrating single-cell transcriptomic data across different conditions, technologies, and species. Nat Biotechnol 2018;36:411–420. [PubMed: 29608179]
74. Tran HTN, Ang KS, Chevrier M, Zhang X, Lee NYS, Goh M and Chen J. A benchmark of batch-effect correction methods for single-cell RNA sequencing data. Genome Biol 2020;21:12. [PubMed: 31948481]
75. Jia C, Hu Y, Kelly D, Kim J, Li M and Zhang NR. Accounting for technical noise in differential expression analysis of single-cell RNA sequencing data. Nucleic Acids Res 2017;45:10978–10988. [PubMed: 29036714]
76. Cao Y, Vergnes L, Wang YC, Pan C, Chella Krishnan K, Moore TM, Rosa-Garrido M, Kimball TH, Zhou Z, Charugundla S, Rau CD, Seldin MM, Wang J, Wang Y, Vondriska TM, Reue K and Lusis AJ. Sex differences in heart mitochondria regulate diastolic dysfunction. Nat Commun 2022;13:3850. [PubMed: 35787630]

77. Cao Y, Wang Y, Zhou Z, Pan C, Jiang L, Zhou Z, Meng Y, Charugundla S, Li T, Allayee H, Seldin MM and Lusis AJ. Liver-heart cross-talk mediated by coagulation factor XI protects against heart failure. Science. 2022;377:1399–1406. [PubMed: 36137043]

78. Shiffler RE. Maximum Z Scores and Outliers. The American Statistician 1988;42:79–80.

Novelty and Significance

What Is Known?

- Heart failure (HF) with preserved ejection fraction (HFpEF) is a common but poorly understood form of HF characterized by impaired diastolic function.
- HFpEF is a highly heterogeneous disorder with multiple comorbidities, including obesity, diabetes and hypertension, and driven in large part by environmental factors.

What New Information Does This Article Contribute?

- Indole-3-propionic acid (IPA) is reduced in HFpEF patients and a mouse model of HFpEF compared with controls.
- IPA supplementation attenuates diastolic dysfunction, metabolic remodeling, oxidative stress, inflammation, gut microbiota dysbiosis, and intestinal epithelial barrier damage in a mouse model of HFpEF.
- IPA improves diastolic and metabolic functions in HFpEF mice by repressing nicotinamide N-methyltransferase (NNMT) and restoring nicotinamide, NAD^+/NADH, and SIRT3 in the heart.
- IPA supplementation shows promise for the prevention or treatment of HFpEF.

HFpEF is a complex disorder with multiple comorbidities and is highly heterogeneous, making human studies difficult. By using a mouse model of the disorder involving feeding mice a high-fat diet and a nitric oxide synthase inhibitor to enable genetic and molecular analysis, we found that indole-3-propionic acid (IPA), a metabolite synthesized by the gut microbe from dietary tryptophan, was decreased in both heart tissue and circulation as compared to a regular diet. IPA attenuated diastolic dysfunction induced by the HFpEF diet and improved metabolic homeostasis. In the hearts of HFpEF mice, IPA restored the expression of SIRT3 by aryl hydrocarbon receptor (AhR) binding and decreased inflammation and NNMT levels, increasing nicotinamide and NAD^+/NADH. To determine the human relevance, we examined two separate cohorts of heart failure patients with HFpEF and the levels of IPA were significantly reduced in HFpEF patients in both cohorts. Our data identifies IPA as a critical regulator of diastolic dysfunction in HFpEF by enhancing the NAD salvage pathway, and support purposing IPA supplementation for therapeutic management against HFpEF.

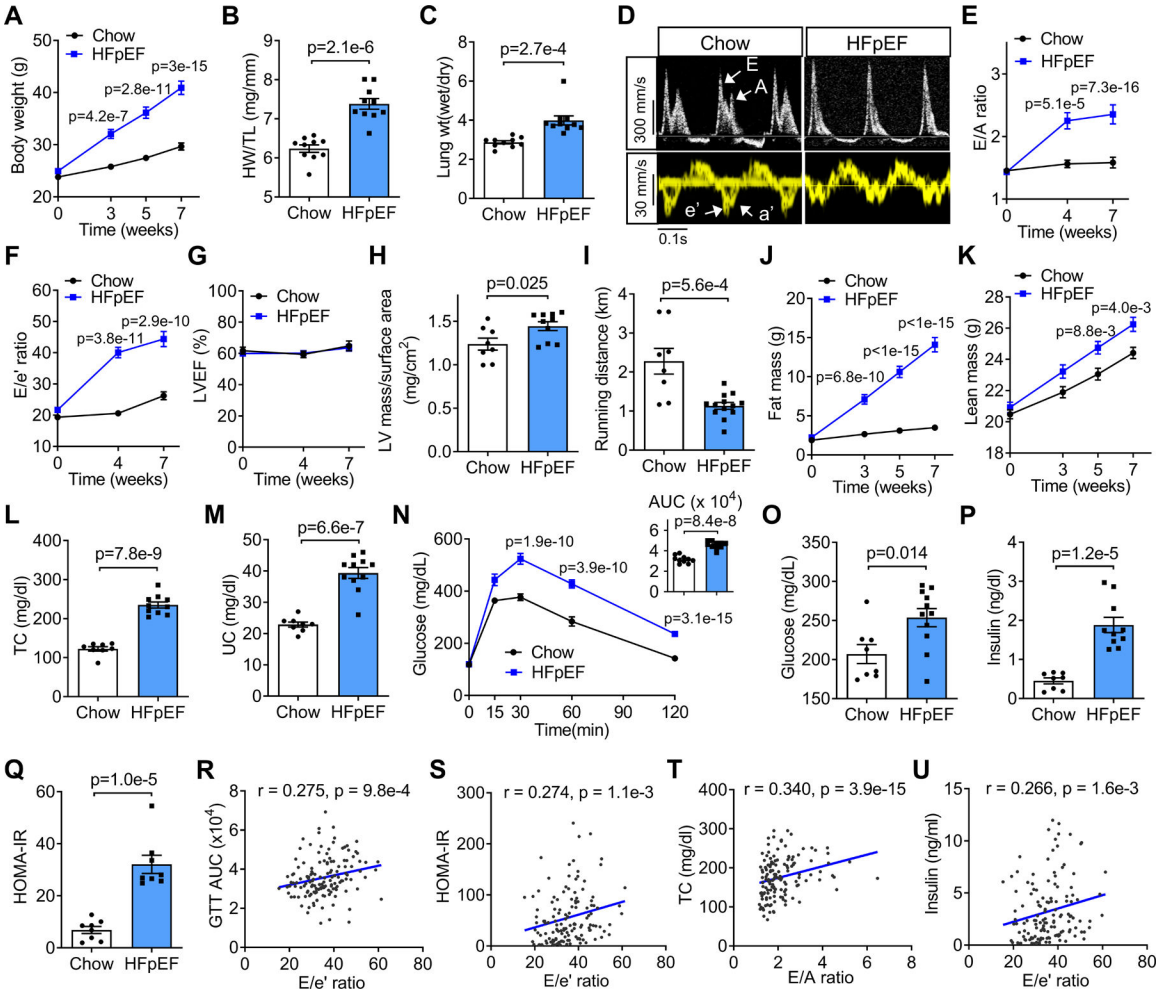

Figure 1. HFpEF mice exhibit metabolic remodeling which is associated with diastolic dysfunction.

C57BL/6J male mice were fed with chow diet or HFD + l-NAME for 7 weeks.

A. Body weight at baseline, weeks 3, 5, and 7. HFD, high-fat diet. n = 10.

B-C. Heart weight/tibia length ratio (**B**) and lung weight (wet/dry ratio, **c**) were measured after 7 weeks of chow diet or HFD + l-NAME. n = 10.

d-h. Representative images of echocardiography (**D**), E/A ratio (**e**), E/e' ratio (**f**), left ventricle ejection fraction (**G**), and left ventricle mass/surface area (**H**) were measured in chow diet (n = 8) or HFD + l-NAME (n = 10) mice.

i. Exercise tolerance test showing total running distance of chow diet (n = 8) and HFD + l-NAME (n = 13) fed mice in a treadmill.

J-K. Fat mass (**J**) and lean mass (**K**) at baseline, weeks 3, 5, and 7. n = 10.

L-Q. Plasma total cholesterol (**L**), unesterified cholesterol (**M**), glucose tolerance test and quantification (**N**), plasma glucose (**O**), insulin (**P**) and calculated HOMA-IR (**Q**) were measured after 7 weeks of chow diet (n = 8) or HFD + l-NAME (n = 11) feeding.

R-U. "Two-hit" HFpEF model was induced in 30 inbred strains of male mice. The correlation between metabolic traits (glucose tolerance, homeostatic model assessment for

insulin resistance (HOMA-IR), plasma total cholesterol, and insulin) and diastolic function traits (E/e' ratio and E/A ratio) were examined. Each dot represents one mouse. Representative of 5 (**A**-**Q**) experiments. Each point represents a mouse. All data are presented as the mean ± SEM. $p<0.05$ are statistically significant and precise values are specified in corresponding figures. ns, no significant. Data were analyzed by Student's *t* test (**B**, **C**, **H**, **I**, **L**-**Q**), by 2-way ANOVA (**A**, **E**, **F**, **G**, **J**, **K**, **N**) or by Spearman's rank correlation (**R**-**U**).

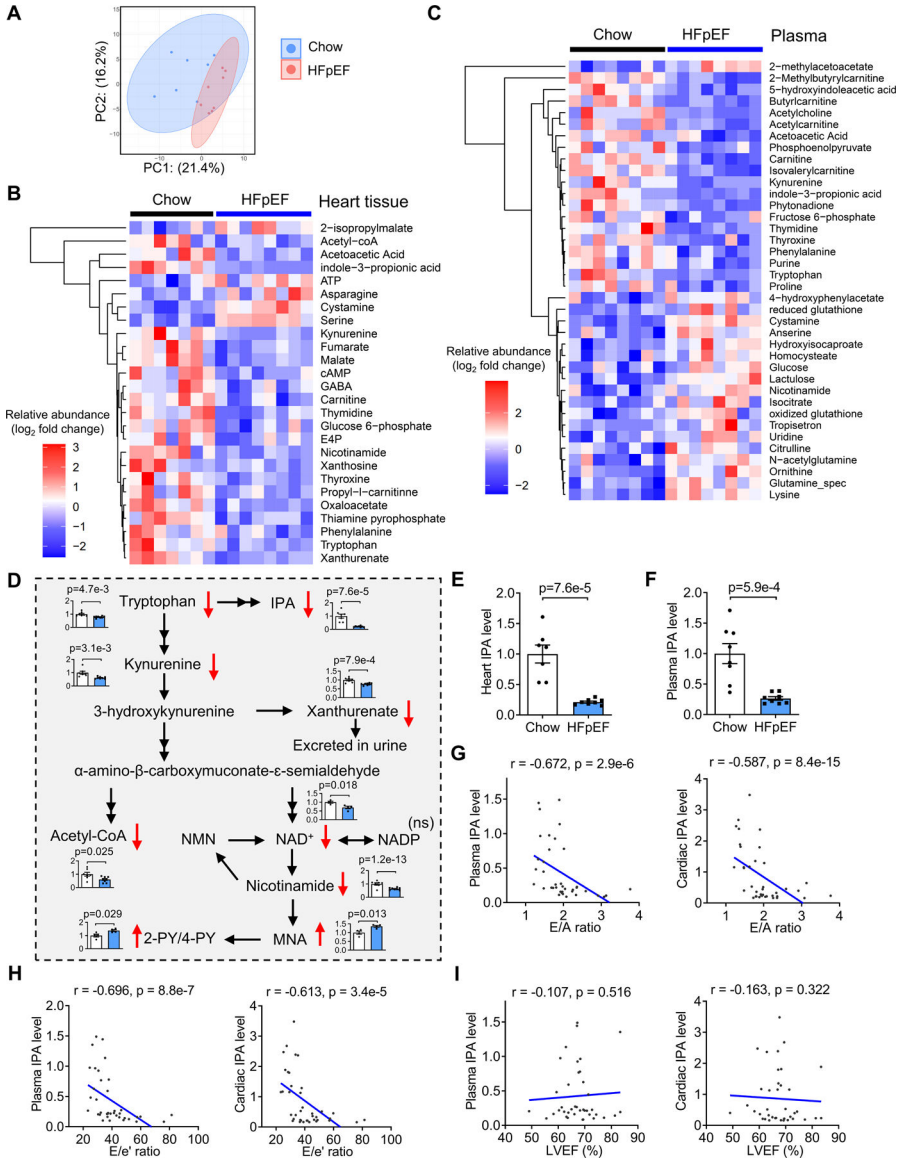

Figure 2. Decreased heart and plasma IPA levels in HFpEF mice.

C57BL/6J male mice were fed with chow diet or HFD + l-NAME for 7 weeks. Heart tissue and plasma were collected for metabolomics.

A. Principal component analysis (PCA) plot of chow and HFD + l-NAME (HFpEF) samples.

B. Heatmap depicting relative abundance of significantly differentiated metabolites in heart tissue from HFpEF (n = 7) versus chow (n = 8) mice.

C. Heatmap depicting relative abundance of significantly differentiated metabolites in plasma from HFpEF (n = 8) versus chow (n = 8) mice.

D. Intermediates in tryptophan metabolism were decreased in the heart from HFpEF mice relative to control mice. Relative abundance of metabolites was shown and the colored bars denote chow (white) and HFpEF samples (blue). Decreased metabolites were denoted with red arrows.

E-I. IPA levels in heart tissue (**E**) and plasma (**F**) of male mice as well as the associations between plasma IPA levels, cardiac IPA levels and diastolic parameters (**G-I**). Representative of 2 (**A-I**) experiments. Each point represents a mouse. All data are presented as the mean ± SEM. $p<0.05$ are statistically significant and precise values are specified in corresponding figures. ns, no significant. Data were analyzed by Student's *t* test (**D**, **E**, **F**), or by Spearman's rank correlation (**G-I**).

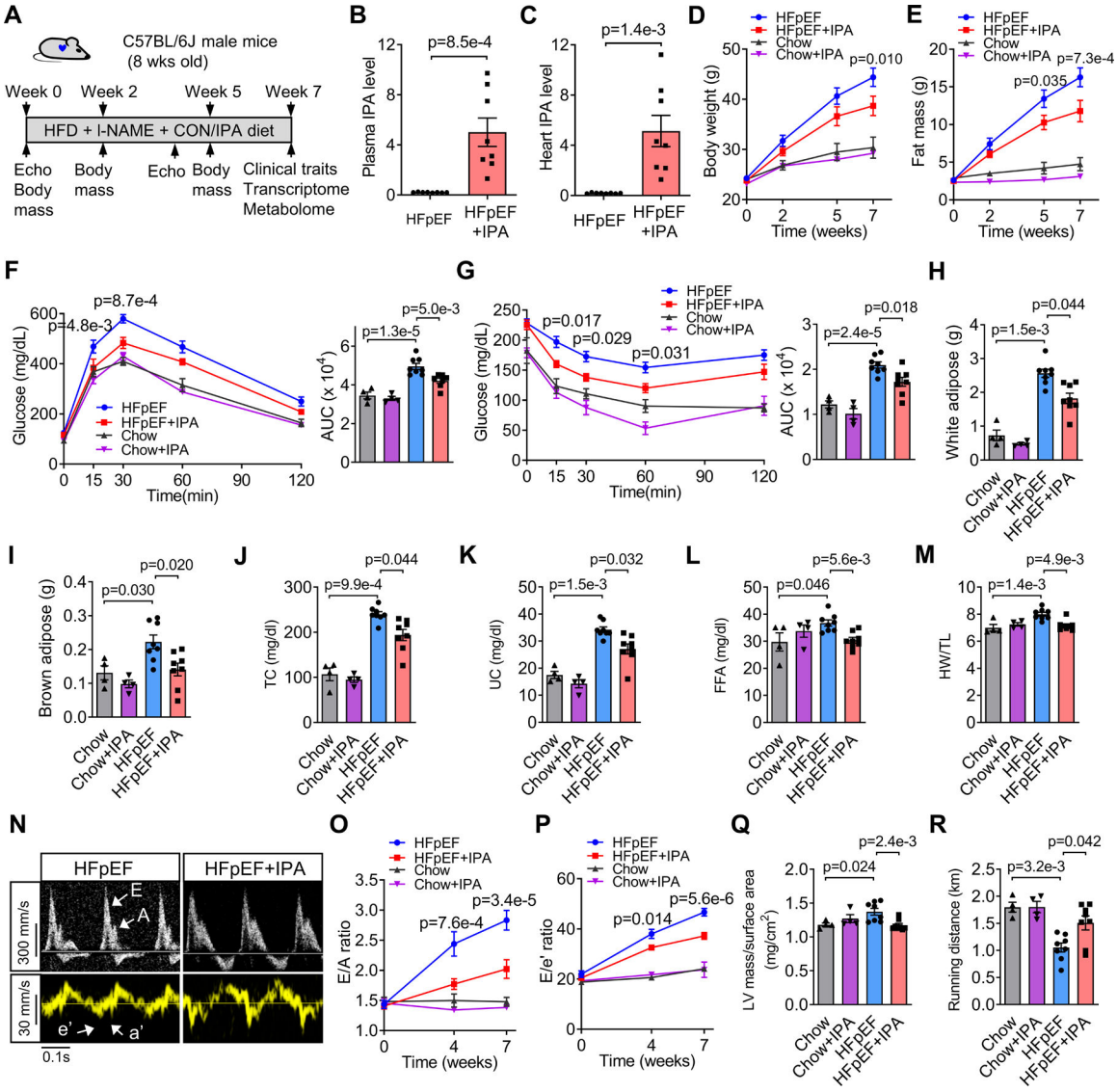

Figure 3. IPA supplementation attenuates diastolic dysfunction and metabolic remodeling.

C57BL/6J male mice (8 weeks old) were fed with chow diet or HFD + l-NAME containing control or high indole-3-propionic acid (IPA, 562.5 mg IPA/kg diet) for 7 weeks.

A. Experimental design.

B-C. Relative IPA levels in plasma (**B**) and heart tissue (**C**) of mice fed with HFD + l-NAME containing control (n = 8) or high IPA (n = 8).

D-E. Body weight (**D**) and fat mass (**E**) at baseline, weeks 2, 5, and 7. n = 4 in Chow and Chow + IPA; n = 8 in HFpEF and HFpEF + IPA.

F-G. Glucose tolerance test (**F**) and insulin tolerance test (**G**) as well as the area under curve (AUC) of the mice after 7 weeks of chow diet or HFD + l-NAME containing control or high-IPA. *P < 0.05 and **P < 0.01 of glucose levels between HFpEF and HFpEF + IPA group. HFpEF and Chow group were significantly different (asterisks shown in AUC). n = 4 in Chow and Chow + IPA; n = 8 in HFpEF and HFpEF + IPA.

H-L. White adipose weights (**H**), brown adipose weights (**I**), plasma total cholesterol (**J**), unesterified cholesterol (**K**), and free fatty acids (**L**) of the mice fed with chow diet or HFD + l-NAME containing control or high-IPA for 7 weeks. n = 4 in Chow and Chow + IPA; n = 8 in HFpEF and HFpEF + IPA.

M-R. Heart weight/tibia length ratio (**M**), representative images of echocardiography (**N**), E/A ratio (**O**), E/e' ratio (**P**), LV mass/surface area (**Q**), and exercise tolerance test (**R**) were measured. Running distance was assessed at the end of feeding and echocardiography was determined at baseline, week 4, and week 7. n = 4 in Chow and Chow + IPA; n = 8 in HFpEF and HFpEF + IPA.

Representative of 4 (**A**-**R**) experiments. Each point represents a mouse. All data are presented as the mean ± SEM. $p<0.05$ are statistically significant and precise values are specified in corresponding figures. ns, no significant. Data were analyzed by Student's *t* test (**B**, **C**), by Kruskal-Wallis test (**H**-**M**, **Q**-**R**), or by 2-way ANOVA (**D**-**G**, **O**-**P**). For **D**-**G** and **O**-**R**, the p values indicate significance between HFpEF and HFpEF + IPA group.

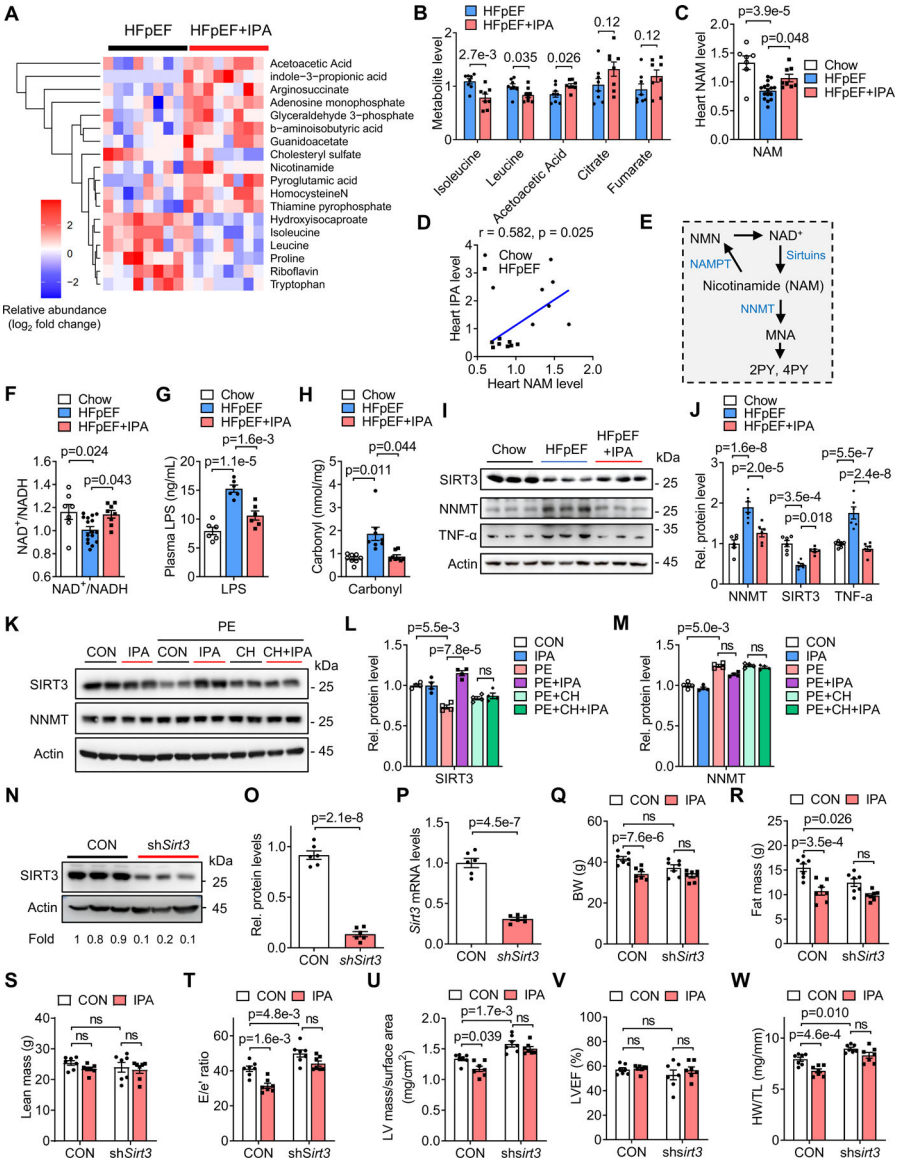

Figure 4. IPA supplementation increases nicotinamide and SIRT3 levels in the heart.

A. Heatmap depicting relative abundance of significantly differentiated metabolites by IPA in the heart of male mice fed with HFD + l-NAME containing control or high-IPA for 7 weeks. n = 8.

B. Relative abundance of indicated metabolites. n = 8.

C. Heart nicotinamide (NAM) level in C57BL/6J male mice fed with chow diet, HFD + l-NAME or HFD + l-NAME containing high IPA for 7 weeks. n = 7 in Chow; n=16 in HFpEF; n = 8 in HFpEF + IPA.

D. Association between heart IPA and NAM levels in C57BL/6J male mice fed with chow diet or HFD + l-NAME. n = 8.

E. NAD salvage pathway.

F. NAD^+/NADH ratio in the heart tissue of mice fed with chow diet, HFD + l-NAME or HFD + l-NAME containing high IPA for 7 weeks. n = 7 in Chow; n=16 in HFpEF; n = 8 in HFpEF + IPA.

G-J. Plasma LPS levels (n = 6) (**G**), protein carbonyl levels (n = 8) (**H**), indicated protein levels (n = 3) (**I**), and protein quantification (**J**) in the heart tissue of mice fed with chow diet, HFD + l-NAME or HFD + l-NAME containing high IPA for 7 weeks.

K-M. Protein levels (**K**), SIRT3 protein quantification (**L**) and NNMT protein quantification (**M**) in HL-1 cells treated with control o1r IPA (1 mM) in the presence of 100 μM phenylephrine (PE) with or without AhR antagonist CH-223191 (5 μM) for 48 hours.

N-P. Protein levels (**N**), SIRT3 protein quantification (**O**) and RT-qPCR (**P**) showing *Sirt3* knockdown in the heart using AAV9-*Sirt3*-shRNA. The relative protein levels were determined by comparing them to the first sample in the control group. The relative mRNA levels were determined by comparing them to the average expression in the control group. n = 6.

Q-W. C57BL/6J male mice (8 weeks old) were injected with control or AAV9-*Sirt3*-shRNA, and fed with HFD + l-NAME or HFD + l-NAME containing high IPA for 7 weeks (n = 7). Body weight (**Q**), fat mass (**R**), lean mass (**S**), E/e' ratio (**T**), LV mass/surface area (**U**), LVEF (left ventricular ejection fraction) (**V**), and heart weight/tibia length (**W**) were measured after the feeding.

Representative of 2 (**A-H, N-W**), 4 (**I**, **J**) and 5 (**K-M**) experiments. Each point represents a mouse. All data are presented as the mean ± SEM. $p<0.05$ are statistically significant and precise values are specified in corresponding figures. ns, no significant. Data were analyzed by Student's *t* test (**B**, **O, P**), by 1-way ANOVA (**C, F-H**), by Spearman's rank correlation (**D**), by Kruskal-Wallis test (**L-M**), or by 2-way ANOVA (**J**, **Q-W**).

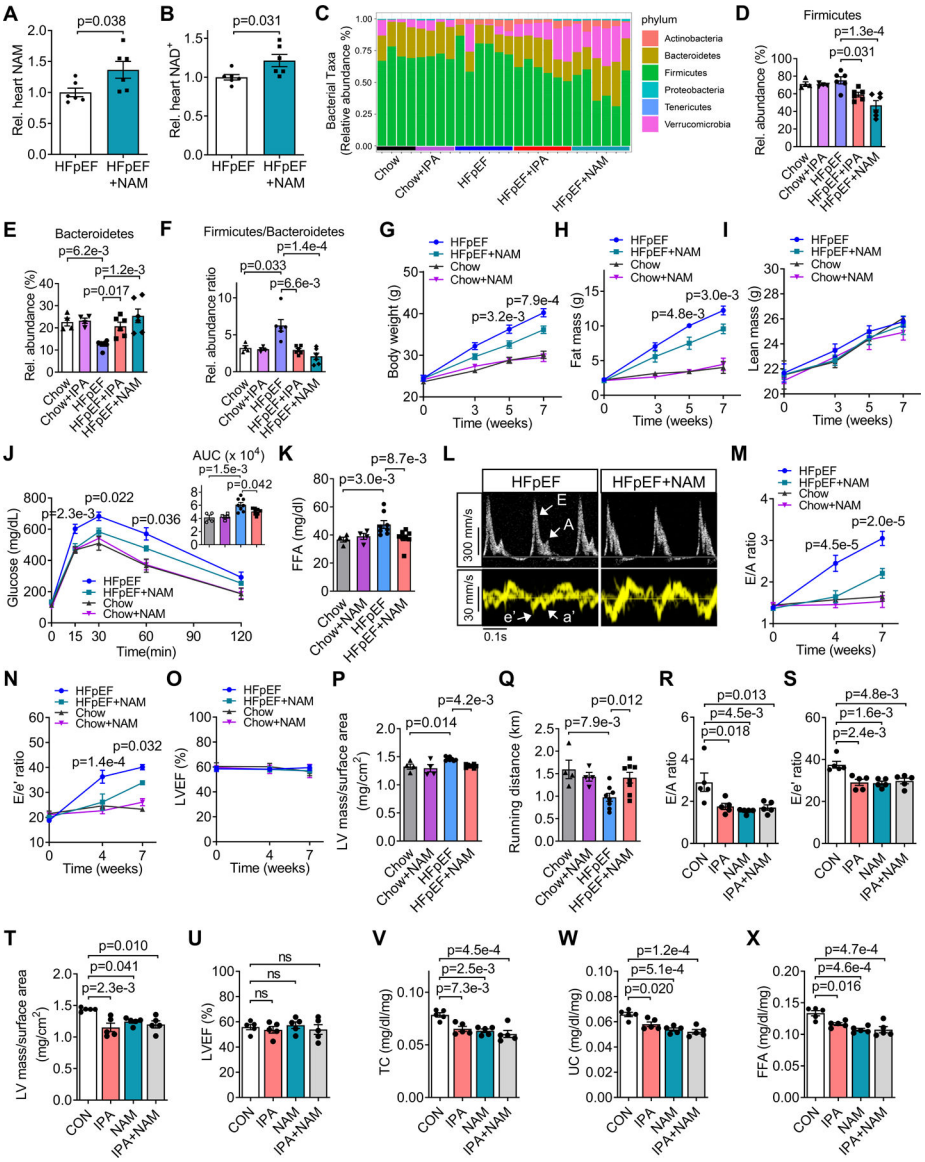

Figure 5. NAM mitigates diastolic dysfunction in HFpEF.

C57BL/6J male mice were fed with chow diet or HFD + l-NAME containing control or high NAM (550 mg/kg/day in drinking water) for 7 weeks.

A-B. Heart NAM (**A**) and NAD^+ (**B**) levels in HFpEF or HFpEF + NAM groups were measured with HILIC (hydrophilic-interaction chromatography) LC-MS. The relative NAM levels were determined by comparing them to the average expression in the HFpEF group. n = 6.

C-F. Cecum samples of Chow, Chow + IPA, HFpEF, HFpEF + IPA, and HFpEF + NAM were collected and 16S rRNA-based gut microbial profiling was performed. Relative abundance of taxa at the phylum level (**C**), relative abundance of Firmicutes (**D**), Bacteroidetes (**E**), and Firmicutes/Bacteroidetes ratio (**F**) in indicated groups were shown. n = 4 in Chow and Chow + NAM; n = 6 in HFpEF, HFpEF + IPA, and HFpEF + NAM.

G-I. Body weight (**G**), fat mass (**H**), and lean mass (**I**) of the mice were measured at baseline, 3, 5, and 7 weeks of feeding with chow diet or HFD + l-NAME containing control or high NAM. n = 4 in Chow and Chow + NAM; n = 8 in HFpEF, and HFpEF + NAM.
J-Q. Glucose tolerance test and quantification (**J**), plasma free fatty acids (**K**), representative images of echocardiography (**L**), E/A ratio (**M**), E/e' ratio (**N**), LVEF (**O**), LV mass/surface area (**P**), and running distance (**Q**) were determined. Echocardiography was performed at baseline, weeks 4 and 7 of the feeding and other parameters were collected after 7 weeks of the diet. n = 4 in Chow and Chow + NAM; n = 8 in HFpEF, and HFpEF + NAM.
R-X. C57BL/6J male mice were fed with HFD + l-NAME containing control, high IPA, high NAM or high IPA + NAM for 7 weeks. E/A ratio (**R**), E/e' ratio (**S**), LV mass/surface area (**T**), LVEF (**U**), heart total cholesterol (**V**), unesterified cholesterol (**W**), and free fatty acids (**X**) were measured after feeding. n = 5.
Representative of 2 (**R-X**) and 3 (**A-Q**) experiments. Each point represents a mouse. All data are presented as the mean ± SEM. $p<0.05$ are statistically significant and precise values are specified in corresponding figures. ns, no significant. Data were analyzed by Student's *t* test (**A**, **B**), by 1-way ANOVA (**R-X**), by Kruskal-Wallis test (**D-F**, **K, P-Q**), or by 2-way ANOVA (**G-J**, **M-O**). For **G-J** and **M-O**, the p values indicate significance between HFpEF and HFpEF + NAM group.

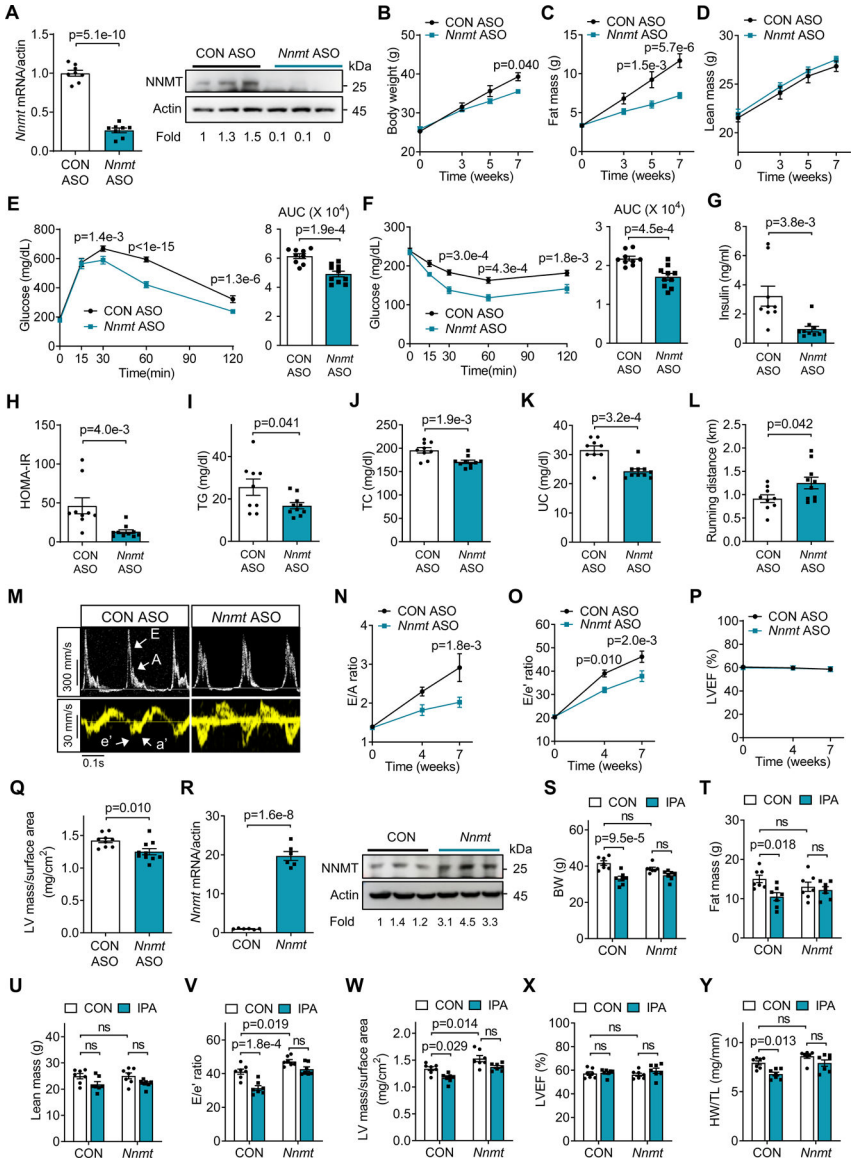

Figure 6. *Nnmt* ASO alleviates diastolic dysfunction in HFpEF.

C57BL/6J male mice were subjected to once-weekly intraperitoneal injection of control or *Nnmt* ASO (an antisense oligonucleotide) and were fed with HFD + l-NAME for 7 weeks.

A. RT-qPCR (n = 8) and Western blotting (n = 3) showing NNMT levels in the heart tissue from mice treated with CON ASO or *Nnmt* ASO. CON, control. The relative mRNA levels were determined by comparing them to the average expression in the control group. The relative protein levels were determined by comparing them to the first sample in the control group.

B-D. Body weight (**B**), fat mass (**C**), and lean mass (**D**) were measured at baseline, weeks 3, 5, and 7 of the feeding in control (n = 9) or *Nnmt* ASO mice (n = 10).

E-Q. Glucose tolerance test (**E**), insulin tolerance test (**F**), plasma insulin (**G**), HOMA-IR (**H**), plasma triglycerides (**I**), total cholesterol (**J**), unesterified cholesterol (**K**), running distance (**L**), representative images of echocardiography (**M**), E/A ratio (**N**), E/e' ratio (**O**),

LVEF (**P**), and LV mass/surface area (**Q**) were measured in control (n = 9) or *Nnmt* ASO mice (n = 10). Echocardiography was performed at baseline, week 4 and 7 of the feeding and other parameters were collected after 7 weeks of feeding.

R. RT-qPCR (n = 6) and Western blotting (n = 3) showing *Nnmt* overexpression in the heart using AAV9-cTnT-*Nnmt*. The relative mRNA levels were determined by comparing them to the average expression in the control group. The relative protein levels were determined by comparing them to the first sample in the control group.

S-**Y**. C57BL/6J male mice were injected with control or AAV9-cTnT-*Nnmt*, and fed with HFD + l-NAME or HFD + l-NAME containing high IPA for 7 weeks (n = 7). Body weight (**S**), fat mass (**T**), lean mass (**U**), E/e' ratio (**V**), LV mass/surface area (**W**), LVEF (**X**), and heart weight/tibia length (**Y**) were measured after the feeding. n = 7.

Representative of 2 (**A**-**Y**) experiments. Each point represents a mouse. All data are presented as the mean ± SEM. $p<0.05$ are statistically significant and precise values are specified in corresponding figures. ns, no significant. Data were analyzed by Student's *t* test (**A**, **E**-**L**, **Q**, **R**), by 1-way ANOVA (**B**-**F**, **N**-**P**), or by 2-way ANOVA (**S**-**Y**).

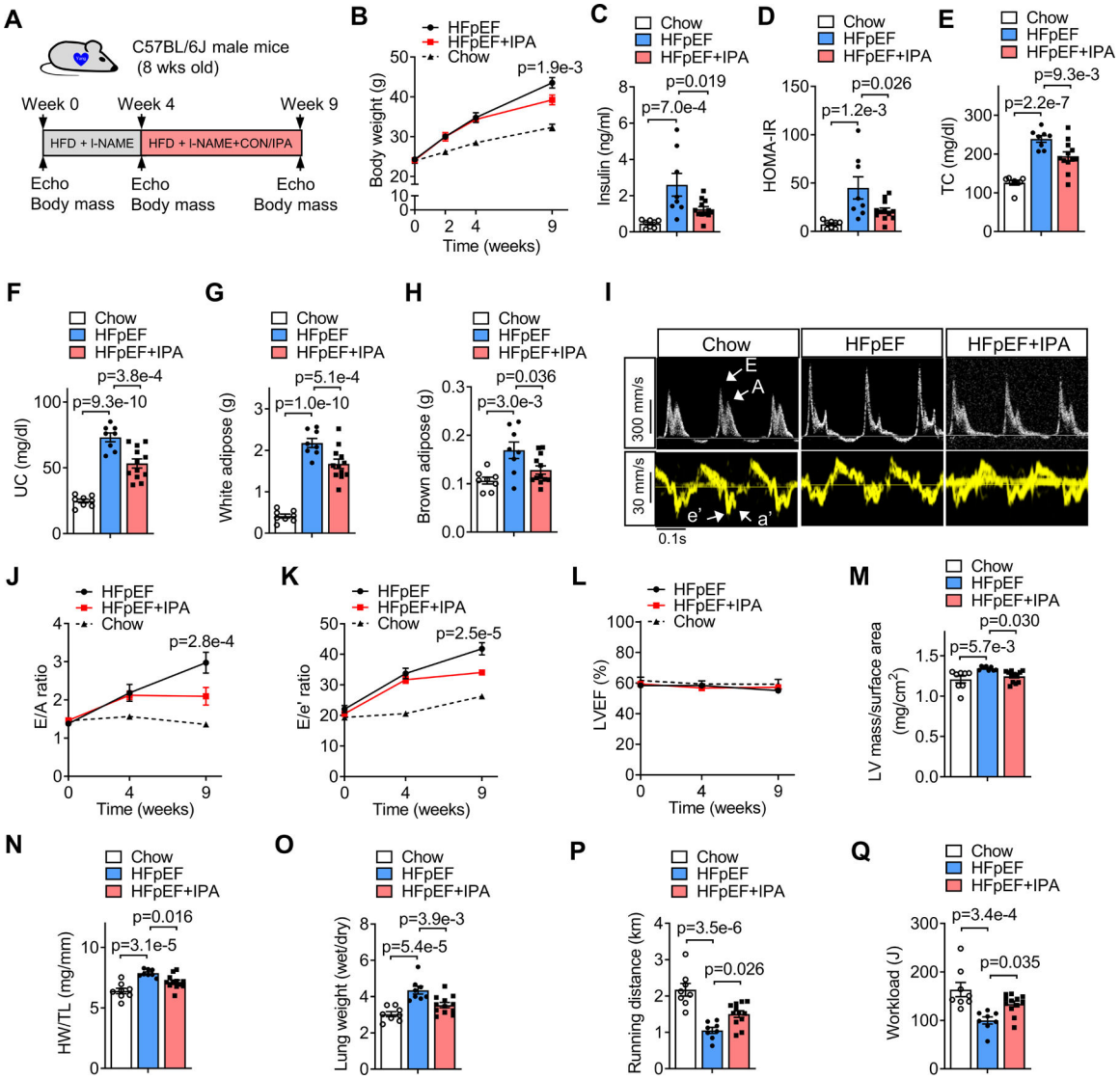

Figure 7. Therapeutic effects of IPA in HFpEF.

C57BL/6J male mice were fed with chow diet or HFD + l-NAME for 4 weeks and followed by control (HFpEF) or high-IPA supplementation (HFpEF + IPA; 562.5 mg IPA/kg diet) for another 5 weeks. n = 8 in chow, n = 8 in HFpEF, and n = 12 in HFpEF + IPA.

A. Experimental design.

B-H. Body weight over time (**B**), insulin (**C**), calculated HOMA-IR (**D**), plasma total cholesterol (**E**), unesterified cholesterol (**F**), white adipose tissue weight (**G**), and brown adipose tissue weight (**H**).

I-Q. Representative images of echocardiography (**I**). E/A ratio (**J**), E/e' ratio (**K**), and LVEF (**L**) over time, LV mass/surface area (**M**), heart weight/tibia length ratio (**N**), lung weight (**O**), exercise tolerance in running distance (**P**) and workload (**Q**) were measured. Representative of 2 (**A-Q**) experiments. Each point represents a mouse. All data are presented as the mean ± SEM. $p<0.05$ are statistically significant and precise values are specified in corresponding figures. ns, no significant. Data were analyzed by 1-way ANOVA

(**B**-**H**, **J**-**Q**). For **B** and **J**-**L**, the p values indicate significance between HFpEF and HFpEF + IPA group.

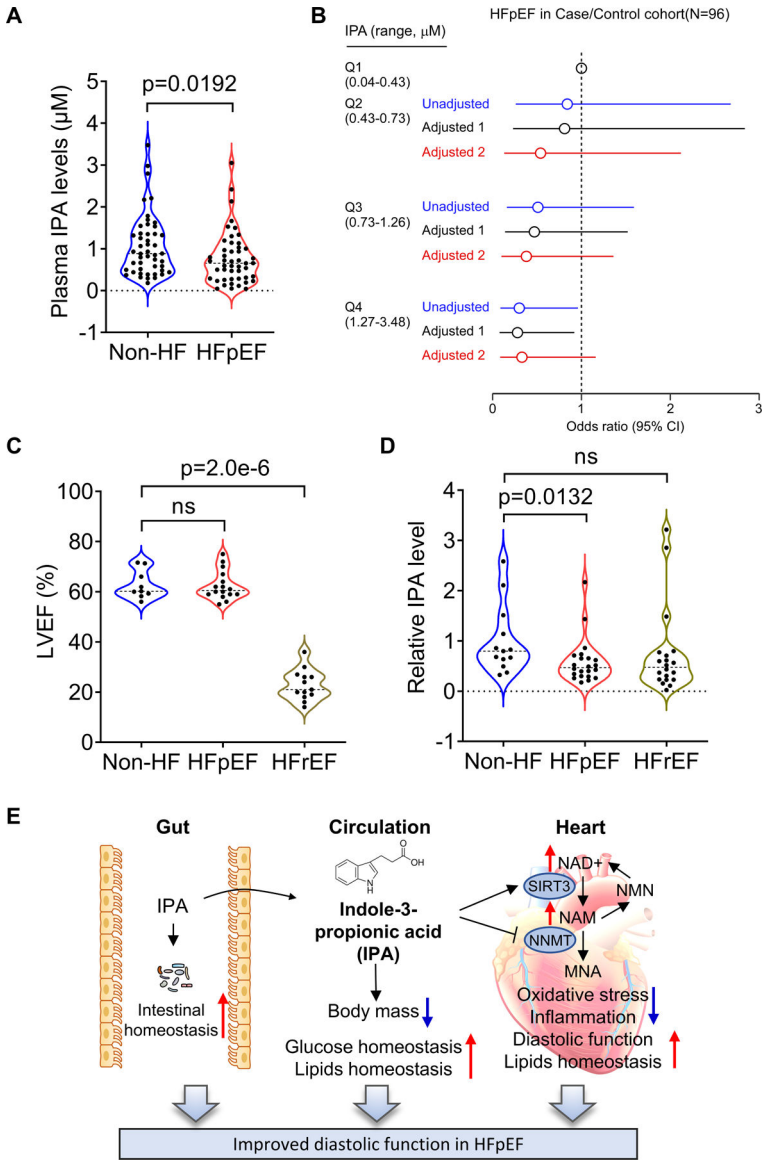

Figure 8. IPA levels are reduced in HFpEF patients but not HFrEF patients

A-B. The association of IPA levels with HFpEF in the Cleveland Clinic HFpEF case/control cohort. (**A**) Violin plots of IPA levels stratified by HFpEF status. Each point represents one patient. Medium is represented by dash line; p value was calculated by Wilcoxon rank sum test. (**B**) Forest plots indicating the odds of HFpEF according to the quartiles of IPA levels using multivariable logistic regression models. Unadjusted odd ratio (blue), Adjusted Model 1 (age, sex, diabetes, hypercholesterolemia, black), Adjusted Model 2 (age, sex, diabetes, BMI and hypertension, red), symbols represent odds ratios and the 5–95% confidence intervals are indicated by line length. n = 48.

C-D. LVEF (**C**) and arterial abundance of IPA (**D**) in non-HF controls (n = 13), HFpEF (n = 22), and HFrEF patients (n = 20) from Alfred Hospital HFpEF study. p value was calculated by Wilcoxon rank sum tests. $p<0.05$ are statistically significant and precise values are specified in corresponding figures. ns, no significant. Each point represents one patient.

E. An illustration summarizing how IPA mediates gut-heart crosstalk in HFpEF. IPA feeding improved gut homeostasis by mitigating gut microbiota dysbiosis and intestinal epithelial barrier damage induced by HFpEF. Thus, metabolic remodeling by the diet was attenuated, including reduced body mass gain, improved glucose levels and lipid homeostasis. In the heart, IPA restored NAM and NAD^+/NADH levels, increased SIRT3 levels and decreased NNMT levels, attenuating oxidative stress and inflammation in the heart. These beneficial effects collectively protect against diastolic dysfunction in HFpEF.